## REJUVENATION OF CRUSTAL MAGMA MUSH: A TALE OF MULTIPLY **NESTED PROCESSES AND TIMESCALES**

FRANK J. SPERA\*,† and WENDY A. BOHRSON\*\*

ABSTRACT. Some relatively crystal rich silicic volcanic deposits, including large volume ignimbrites, preserve evidence of a history where a rheologically locked high crystallinity magma was rejuvenated (unlocked) through enthalpy (± mass) exchange with newly injected recharge magma of higher specific enthalpy. This is one event in a possible complex history. That is, the volcanic product of an eruption reflects an array of sequential and nested processes including melt formation and segregation, ascent, cooling, crystallization, crustal assimilation, magma recharge, unlocking, shallow ascent, fluid exsolution, and eruption. Deconvolution of these these nested processes and concomitant timescales is complicated and relies on a multidisciplinary approach; studies that do not clearly associate process and correlated timescale have the potential to provide misleading timescale information. We report the results of thermodynamic and heat transfer calculations that document mass, energy, and phase equilibria constraints for the unlocking of near-solidus rhyolite mush via magma mingling (heat exchange only) with basaltic recharge magma of higher specific enthalpy. To achieve unlocking, defined as the transition from near-solidus to  $\sim 50$  percent melt of the host silicic magma, phase equilibria computations provide (1) the enthalpy required to unlock mush, (2) the mass ratio of recharge magma to mush (M<sub>R</sub>/M<sub>M</sub>) when the two magmas achieve thermal equilibrium, and (3) the changes in melt, mineral, and fluid phase masses, compositions, and temperatures during the approach to unlocking. The behavior of trace elements is computed with knowledge of mineral, fluid, and melt proportions and solid-fluid and solid-melt partition coefficients. Evaluation of unlocking for relatively 'dry' (0.5 wt. % H<sub>2</sub>O) and 'wet' (3.9 wt. % H<sub>2</sub>O) rhyolitic mushy (locked) magma by basaltic recharge at upper crustal pressures indicates minimum values of  $M_R/M_M$  can be significantly less than 1, assuming the mingling process is isenthalpic with no 'waste' heat. For active volcanic systems estimates of M<sub>R</sub> may be tested using geodetic data. Wet mush has lower energy requirements for unlocking and thus requires lower  $M_R/M_M$  than dry mush. Wet rejuvenated magmas therefore may be more abundant in the volcanic rock record, and unlocked dry mushes may be restricted to extensional tectonic settings with high recharge flux. Temperature changes in dry mush as it unlocks are pronounced (greater than 150 °C) compared to those in wet mush, which are smaller than the resolution of classical geothermometry ( $\sim$ 15 °C). Phase equilibria calculations show that, as required, the net volume of crystals decreases during unlocking. Interestingly, calculations also indicate reactive crystal growth by chemical re-equilibration at the crystal-size scale during unlocking may also take place. In either dissolution by unidirectional resorption or reactive dissolution/ new growth, the chemical signatures of unlocking, potentially preserved in crystals or parts of crystals (for example, rims), are predictable and hence testable. Independent of unlocking thermodynamics, the phase equilibria and elemental consequences of isentropic magma ascent, a transport event that follows unlocking, can also be predicted; detailed examination of several canonical cases reveals a marked contrast with isenthalpic unlocking, thereby providing a means of process deconvolution. Unlocking timescales are estimated by two methods, one that calculates the time to reach thermal equilibrium for recharge magma dispersed in mush as 'clumps' of fixed size, and the second where the required volume of recharge magma is initially a single clump and evolves to smaller size through clump stretching and folding. For a range of

<sup>\*</sup> Department of Earth Science & Earth Research Institute, University of California, Santa Barbara, California 93106, spera@geol.ucsb.edu

<sup>\*\*</sup> Department of Geological Sciences, Central Washington University, 400 E. University Way, Ellensburg, Washington 98926, bohrson@geology.cwu.edu Corresponding author: spera@geol.ucsb.edu

magma volumes from 0.1 to  $5000~\rm km^3$ , unlocking times range from  $10^{-2}$  to  $10^6$  years. The shorter timescales for any magma volume requires a large number of relatively small clumps ( $n > 10^6$ ), which implies that large volumes of mush purported to unlock over short timescales ( $10^2 - 10^3$  years and less) should preserve and exhibit evidence of intimate magma mingling. The key result of our analysis is that multiple timescales are operative during the potentially long and complex history of silicic mush formation, rejuvenation, and ascent. To correctly ascribe timescales to unlocking requires a holistic understanding of the myriad processes that affect the magma before, during, and after enthalpy exchange. In the absence of this context, unlocking timescales may be incorrectly constrained which, in turn, may hinder eruption forecasting and associated hazard mitigation.

Keywords: mush defrosting, magma thermal rejeuvenation, magma mingling, mobilization of mush, thermodynamics of magma rejeuvenation

#### INTRODUCTION

On the very first page of his classic 1928 monograph, The Evolution of Igneous Rocks (Bowen, 1928), N.L. Bowen made reference to the then extant idea that intermediate composition plutonic and volcanic rocks (diorites, granodiorites, andesites and dacites) could be generated by the mixing (chemical and thermal) of pre-existing basaltic and rhyolitic magmas (for example, Bunsen, 1851). Bowen then went on to say "this [hypothesis of mixing] has been found to fail so completely that the concept of differentiation has come to be regarded as a fact". Bowen, of course, championed fractional crystallization as the fundamental petrogenetic process responsible for the diversity of igneous rocks, a viewpoint that remains popular today. During and around the years of Bowen's revolutionary studies (1915–1937), however, debate continued regarding the relative importance of magma mixing (recharge), assimilation and differentiation by fractional crystallization in petrogenesis. Indeed, the eminent geologist Reginald Daly authored a paper in this journal (Daly, 1905) over a century ago arguing for the quantitatively significant role of assimilation of country rock in the petrogenesis of certain granites and related igneous rocks. Although Daly accepted that differentiation by fractional crystallization was important, he also argued that assimilation, especially by wallrock stoping and associated assimilation of partial melts from country rock, was a significant petrogenetic process in his cogently explicated treatise Igneous Rocks and Their Origin (Daly, 1914). His arguments were based on field observations and whole rock compositions. From the modern vantage, one is struck by the quality of these earlier discussions (1850–1930) and by the early implicit realization that the processes of magma mixing, assimilation, and differentiation (by fractional crystallization) are not mutually incompatible. In addition, a closed system is not a prerequisite for a significant role to be ascribed to fractional crystallization. Nowadays, instruments including electron and ion microprobes, mass spectrometers, digital image analysis software, lasers, cold and heating stages and remote sensing devices are routinely used to probe in detail the spatiotemporal record of petrologic processes recorded in melts, crystals, volcanic gas emissions, melt and fluid inclusions from plutonic and volcanic rocks. Based upon high spatial resolution studies of multiple magmatic systems spanning a wide range of eruptive and intrusive volumes, compositions, and emplacement or storage depths, using the tools of modern isotope and trace element geochemistry, petrology, geochronology, phase equilibria, and magma dynamic modeling, we can assert a century after Bowen's first classic paper, The Later Stages of the Evolution of the Igneous Rocks (Bowen, 1915) that magmatic systems generally evolve not as isolated closed systems (that is, by only fractional crystallization) but instead as open systems that profoundly exchange heat, matter, and momentum with their surroundings during a protracted life span that involves the nested processes of melt generation, segregation, ascent, storage, magma mixing, cooling, crystallization, contamination,

re-heating and sometimes eruption, not necessarily in the order listed here. That is, in addition to the important effects of fractional crystallization, processes including the assimilation of wallrock partial melts and/or reaction of country rock with resident magma by stoping, as well as the recharge and mixing of magmas (Wilcox, 1999) are now also unambiguously established as major petrogenetic processes. The challenge in the 21<sup>st</sup> century is to unravel the complicated signals preserved in the igneous record in order to determine or constrain the relative importance, chronology and depths at which these mechanisms operate at specific magmatic centers. The collective insights gained by detailed studies at many magmatic centers will eventually provide the information to develop a petrogenetic 'taxonomy' of magma transport systems, especially their frequencies in different petrotectonic environments.

One of the most challenging tasks is to document the physical and chemical states of magma bodies that feed eruptions. Of particular interest are those magmatic systems that have the potential to yield large and highly explosive eruptions. In the past 25 years, the image of a magma body as a long-lived melt-dominated chamber has given way to one in which magma bodies undergo transients in crystallinity with some spending significant amounts of time in a near-solidus state. This change in perception began first with consideration of magmatic systems in oceanic environments, specifically along the 75,000 km globe-encircling mid-ocean ridge basalt (MORB) magma system (for example, Sinton and Detrick, 1992) and more recently in intermediate to silicic continental crustal magmatic systems (for example, Mahood, 1990). Here, we focus solely upon the latter, although the ideas discussed can be applied with some caveats to MORB systems as well. The essential concept is that via magma recharge and concomitant heat transfer, highly crystalline, rheologically "locked" very viscous magma undergoes thermal rejuvenation (or unlocking), a necessary precursor to eruption. While the literature is replete with studies that document a range of aspects of unlocking (enthalpy transport, magma mixing, phase equilibria consequences, melt extraction, timescales . . . see Background section), many of these studies are focused on specific systems or single out a specific detailed mechanism. In this study, our goal is to present a perspective of processes and timescales associated with rheological unlocking by the apposition of hot, generally more mafic, melt-dominated recharge magma with a resident (locked) crystal mush. For near-solidus rhyolitic mush (hereafter labeled M) and basaltic recharge (hereafter labeled R), we document the energy requirements, phase equilibria, and trace element consequences of unlocking, and roughly evaluate unlocking timescales based on the intimacy of thermal exchange using two simplified transport models. Variables such as bulk composition and relative masses of M and R, the interfacial surface across which heat can be exchanged, and progress towards the attainment of chemical potential equilibrium all influence the composition, crystallinity, and thermal state of the silicic mush. These, in turn, define timescales for the exchange of heat needed to unlock crystal-rich magma by renewed partial melting. Through constraints imposed by mass and energy balance, we define processes associated with unlocking, quantify a range of unlocking timescales, and emphasize how these timescales should be placed in context with a chronology of unlocking, ascent, and eruption.

## BACKGROUND ON SILICIC MAGMA REJUVENATION

Intermediate to silicic crustal magmas with average crystallinity ranging from 50 to 60 percent behave as high-viscosity granular materials with apparent shear viscosities in the range 10<sup>14</sup>–10<sup>18</sup> Pa s (for example, Lesher and Spera, 2015). Rheologically locked magma (Marsh, 1981; Miller and Wark, 2008) has a low probability of eruption unless mechanically disrupted at very shallow depths by fracture induced by expansion of volatiles. The precise value of the threshold melt fraction at which unlocking occurs depends on the abundance, size, and shape distribution as well as the three-

dimensional spatial distribution of crystals within the multiphase magmatic mixture (for example, Moitra and Gonnermann, 2015) and secondarily by the viscosity of the interstial melt. The study of 'jamming' rheology, that is, the phenomenon whereby a disordered two-phase (solid-melt) material becomes rheologically locked when the fraction of solid passes a threshold, dates from the time of J.D. Bernal and his famous experiments (Bernal's Balls) dealing with the packing of hard spheres (Bernal, 1959; Finney, 2013). For a random packing of equant monodisperse crystals, the average unlocking fraction is in the range 50 to 60 volume percent solid or 40 to 50 volume percent melt. For concreteness, in this work, we adopt 50 mass percent melt separating the locked and unlocked rheological states. Although this study focuses upon unlocked magmas that erupt, the concept has also been applied to plutonic systems in the context of the origin of mafic enclaves. In the plutonic realm, physical evidence for unlocking is based upon field studies and thermal modeling of the unlocking process frozen in time and preserved in the geologic record (for example, Pabst, 1928; Reid and others, 1983; Furman and Spera, 1985; Vernon, 1990; Didier and Barbarin, 1991; Wiebe, 1996; Baxter and Feely, 2002).

Examples of formerly locked magmatic systems proposed to have undergone unlocking and eruption include Mt. Pinatubo, Mt. Unzen, Fish Canyon Magma Body, and Mount St. Helens (Pallister and others, 1992; Nakamura, 1995; Bachmann and others, 2002; Claiborne and others, 2010; respectively). Commonly, these unlocked volcanic deposits exhibit internal textural and chemical features indicative of a parental magma that earlier possessed a greater crystallinity (for example, Bachmann and others, 2002; Zellmer and others, 2003; Wotzlaw and others, 2013; Klemetti and Clynne, 2014). A reasonable interpretation of the change in magma's rheological state is that its crystallinity decreased before eruption through injection of new magma (or associated volatiles) that decreased the solidus temperature of the mush by transfer of heat or volatiles (or both) to the mostly crystalline mush (for example, Mahood, 1990; Bachmann and Bergantz, 2006; Huber and others, 2010; Burgisser and others, 2011; Huber and others, 2011; Pistone and others, 2013; Parmigiani and others, 2014). In this study, attention is focused upon this process of thermal rejeuvenation. Evidence for reheating in volcanic deposits supports this idea (for example, Wark and others, 2007; Molloy and others, 2008), as do studies of silicic plutons (for example, Wiebe and others, 2004; Claiborne and others, 2010). Unlocking timescales are a pointed subject of interest, not the least because they potentially inform volcanic eruption prediction and associated hazard mitigation (for example, Wark and others, 2007; Wotzlaw and others, 2013; Klemetti and Clynne, 2014; Till and others, 2015). Vigorous debate about all aspects of magma rejuvenation—the phase equilibria consequences, mechanisms of heat transfer, sources of enthalpy, timescales, role of volatiles, indeed, even the efficacy of the model for all silicic systems—has been ongoing for a few decades [see Bachmann and Huber (2016) for a recent summary of ideas related to mushes, and Streck (2014) for some counter arguments about the applicability of mush extraction models], and will continue to evolve in response to constraints provided by field and analytical data, computational modeling, and experiments. One of the goals of the present work is to provide a bird's eye perspective and emphasize possible tests of the unlocking hypothesis.

#### UNLOCKING SILICIC MAGMAS: CHRONOLOGY OF PROCESSES AND DIVERSITY OF TIMESCALES

In order to provide context for the myriad processes that lead a magma body to an unlocked and potentially eruptible state, figure 1 is offered as a schematic illustration. It summarizes the range of petrologic and other processes, mass and enthalpy exchange opportunities, and qualitative timescales that may characterize magma as it forms and segregates in the mantle, and ascends through and is stored in the crust,

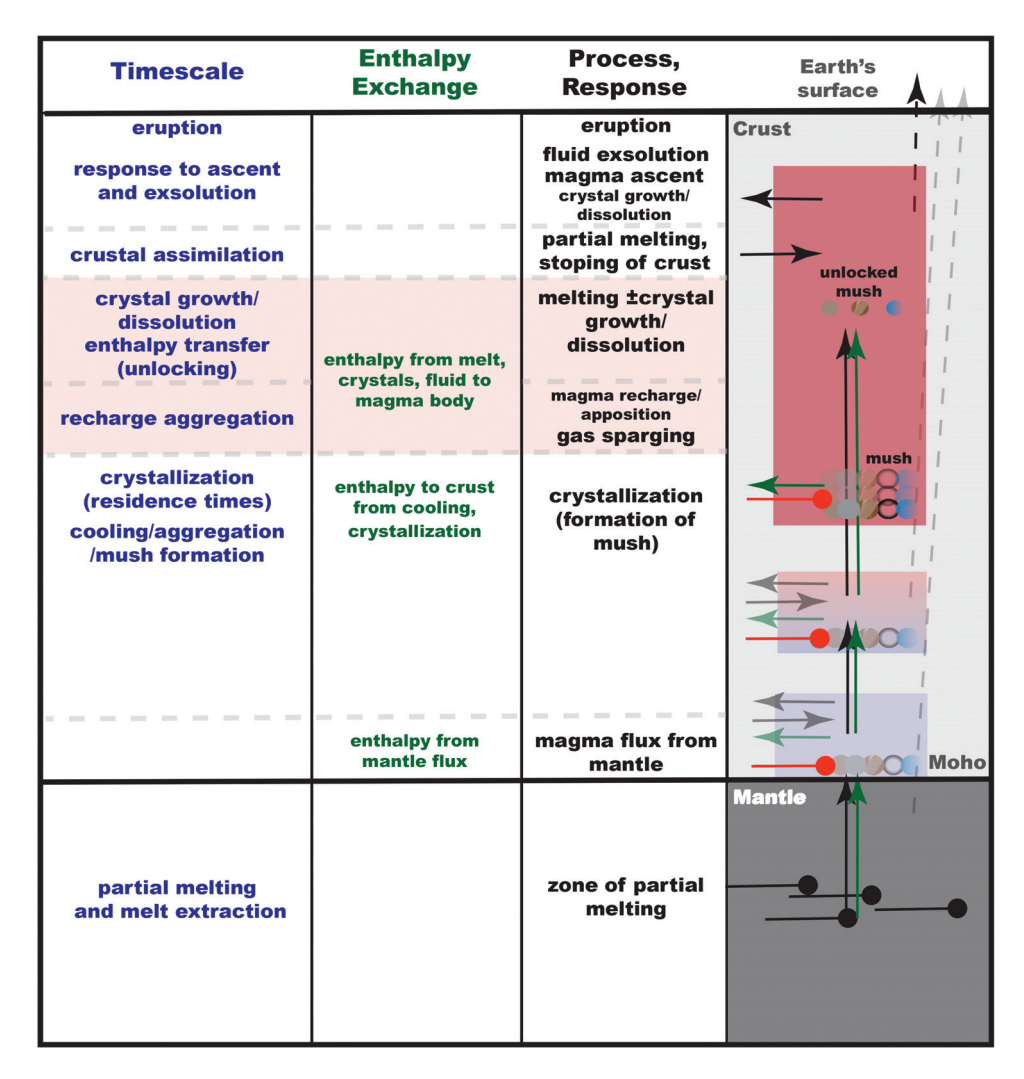


Fig. 1. Schematic illustration of processes (listed in black), heat exchange (listed in green), and qualitative timescales (listed in blue) involved in origin and evolution of silicic magma. Zone of partial melting in mantle represented by black ball and stick symbols; cumulate/mush represented by red ball and stick symbols and small circles; unlocked mush represented by sparse circles. Black arrows represent mass transfer (for example, recharge); green arrows represent heat transfer into magma from recharge, from magma to crust); black and gray arrows represent mass exchange into magma/mush from assimilation and fluid exsolution from magma. Arrows to surface represent schematic eruption paths. Processes and enthalpy exchange principally associated with unlocking process highlighted by pale red box include: aggregation of recharge magma that mingles with mush; enthalpy transfer from recharge magma to mush; associated phase equilibria response (growth, resorption, reaction of crystals, formation of melt). Timescales include recharge aggregation, enthalpy transfer (defined here as unlocking), and a variety of possible timescales associated with crystals. Illustration not to scale.

where it may achieve a near-solidus state by cooling and crystallization. This crystalladen mush may then be thermally rejuvenated and perhaps erupted.

While the origin and evolution of a particular batch of rhyolitic magma can be debated—with distinctions in the balance among crystallization, magma mixing/recharge, crustal assimilation, degassing, and other processes—most petrologists agree that the ultimate source of magma is partial melt from the mantle. Formation and

extraction of mantle melt (and the associated timescales) are early but necessary steps in forming silicic magmas. This deep-seated record is typically difficult to unravel due to later obfuscating effects. Mantle processes and timescales are not discussed further in this study. As shown by a multitude of studies, particularly those that document zircon ages and chemical signatures, many silicic magma bodies aggregate and compositionally evolve over timescales of 10<sup>4</sup> to 10<sup>6</sup> years (for example, Coleman and others, 2004; Vazquez and Reid, 2004; Bacon and Lowenstern, 2005; Miller and others, 2007; Claiborne and other, 2010; Eddy and others, 2016), although much shorter timescales are implicated in other studies (for example, Schmitt, 2006; Braggagni and others, 2014; Pamukcu and others, 2015). Rates of magma generation in the range 10<sup>-2</sup> km<sup>3</sup>/yr to 10<sup>-4</sup> km<sup>3</sup>/yr are consistent with 10 ka to Ma durations for accumulation of  $\sim 100 \text{ km}^3$  of magma. Depending on the thermal conditions of the crust (for example, rate of magma recharge, geothermal gradient, depth of magma storage, vigor of associated hydrothermal system), size of the magma body, and the presence or absence of eruption catalysts, magma may cool to near solidus (or below) conditions, where it spends some, perhaps large, proportion of its history (Cooper and Kent, 2014) as a rheologically locked mush. Some of these bodies never erupt but instead solidify as intrusions (for example, Wiebe and others, 2004). In other cases, there is evidence that these mushes undergo sufficient 'defrosting' to rheologically unlock. Such systems have higher eruption probabilities compared to their frozen antecedents. This rheological transformation, which involves increasing the melt fraction of ambient magma, most likely occurs through recharge of magma that is often but not exclusively basaltic (for example, Druitt and others, 2012); volatiles may also play a key role (Bachmann and Bergantz, 2006, Pistone and others, 2013). There is a minimum mass of apposed recharge magma that must underplate and/or mix with mush in order to satisfy the energy (enthalpy since the process is approximately isobaric) requirement of unlocking. Associated with this period of recharge "aggregation" is a timescale. In the case of underplating with no mass exchange, there is an unlocking timescale associated with heat conduction from the mafic magma into the mush. If the basal molten region within the mush becomes thick enough, convection may become the dominant mechanism of heat transport (Madruga and Curbelo, 2017). If mass exchange occurs (melt, crystals, fluid phase) between mush and recharge magma, then there is an (unlocking) mixing timescale that includes both mass and enthalpy transfer. As enthalpy is added to the mush, changes to phase abundances and compositions will occur as dictated by the phase equilibria; mush temperature may or may not substantially increase. A dominant response to enthalpy addition is mineral dissolution, which occurs over a timeframe dictated not only by the rate of enthalpy addition to the mush but also by thermodynamics (phase equilibria constraints) and kinetics of resorption (phase dissolution). During dissolution, reactive re-equilibration between crystal and melt may change crystal chemistry; this process also has a characteristic timescale that is controlled by diffusion and interface kinetics. In some cases, crystal growth may occur during enthalpy addition, and, like resorption, its timescale will be a function of phase equilibria and kinetic constraints. Each element in each mineral phase will have its own (complicated) history (Cottrell and others, 2002), and therefore, timescales represented by dissolution or growth of individual phases, a mm scale process, will not necessarily be the same as that of unlocking of large volumes (0.1-1000's km<sup>3</sup>) of formerly locked magma via enthalpy transfer. If unlocking is primarily due to addition of H<sub>2</sub>O, its dispersion within the mush is yet another unlocking timescale to consider. During or after thermal exchange and the associated phase equilibria responses, magma may undergo decompression and ascent. Further phase equilibria changes may occur, including crystal growth ± resorption ± fluid exsolution. These events record post-unlocking timescales because the very last stages leading up to eruption

(decompressive rapid ascent) are approximately isentropic (polybaric) decompressive and do not reflect defrostive rejuvenation which is approximately an isenthalpic-isobaric process. If the magma indeed reaches Earth's surface, then there is a timescale associated with eruption, emplacement and cooling, which is not considered in this study.

This chronology illustrates, from a bird's eye perspective, that a number of nested processes and timescales can attend 'unlocking.' Each process that occurs has its own timescale, and the challenge is to associate notable features of the mineralogical, petrological, geochemical, and geochronological record with specific processes, being careful not to conflate phenomena. Failure to correctly associate process and timescale has the potential to yield inchoate (or worse, incorrect) interpretations of unlocking timescales. The claim that large volumes of silicic magma can be unlocked on timescales of order years to decades needs to be supported by more than one line of evidence; partial diffusive re-equilibration of a reaction rim, for example, is not necessarily sufficient to define an unlocking time in isolation.

# ENERGETIC, PHASE EQUILIBRIA, AND ELEMENTAL CONSTRAINTS ON UNLOCKING AND DECOMPRESSING RHYOLITE MUSH

Our approach to examining the consequences of unlocking involves assessing enthalpy and phase equilibria implications of partially melting  $\bf M$  mush of rhyolitic ( $\sim 71.5$  wt. %  $\rm SiO_2$ ) bulk composition via thermal exchange with  $\bf R$  recharge magma of basaltic composition ( $\sim 45$ . wt. %  $\rm SiO_2$ ). In our discussion below, we define the unlocked state as  $\sim 50$  percent in the  $\bf M$  magma but report results to 100 percent melt. The energetic, phase equilibria, and elemental consequences of partially melting sub-solidus rhyolite isobarically to an unlocked state (and beyond) are discussed below, including the strategy for computing these constraints. We also compare the consequences of unlocking with those of isentropic ascent of magma. For brevity, we focus on four specific cases: wet and dry mushes at 0.1 and 0.3 GPa. Many other cases can be studied; the tools to perform the phase equilibria computations are widely available.

#### Strategy for Energetic, Phase Equilibria and Major and Trace Element Calculations

Rhyolite-Melts (Gualda and others, 2012; Ghiorso and Gualda, 2015) version 1.2.0 produced the phase equilibria, major element, and enthalpy constraints for unlocking reported in this work. Trace element results utilized the equilibrium melting equation in Spera and others (2007), with mineral-melt distribution coefficients chosen from those listed in the Geochemical Earth Reference Model (GERM) database. Bulk K<sub>sm</sub> (solid-melt) coefficients were calculated for each relevant step of the partial melting process, given solid-melt partition coefficients and proportions of phases. Because their range is large, two sets of solid-melt partition coefficients were chosen; the first represents values that were among the highest for all relevant minerals, and the second represents values that were among the lowest. Wherever possible, the chosen  $K_{sm}$  were limited to those listed for rhyolite, high Si rhyolite, or low Si rhyolite in the GERM database. Quartz was not among the reported minerals for any element, and its K<sub>sm</sub> was arbitrarily set at 0.001. Additional details about K<sub>sm</sub> are discussed below and listed in table 1. Two bulk K<sub>sf</sub> (solid-fluid) distribution coefficients were chosen (0.001 and 1000) to provide end-member limits on the partitioning of elements during melting. Large values of K<sub>sf</sub> correspond to elements that are not soluble in supercritical H<sub>2</sub>O-rich magmatic fluids; small values imply a large fluid solubility.

Two examples of rhyolite equilibrium melting are presented, with initial (liquidus)  $H_2O$  concentrations of 0.5 weight percent to reflect a relatively dry system and  $\sim$ 3.9 weight percent to reflect a nearly saturated system at 0.1 GPa. These two models are referred to as "dry" and "wet", respectively, in the remainder of this work. The basalt that provides the required heat has  $\sim$ 2.7 weight percent initial (liquidus)  $H_2O$ ,

Mineral-melt Partition Coefficients Used in Normalized Trace Element Calculations TABLE 1A

Element	Plagioclase Ksm	K <sub>sm</sub> Alkali feldspar K <sub>sm</sub>	Orthopyroxene K <sub>sm</sub>	Spinel K <sub>sm</sub>	Spinel K <sub>sm</sub> Ilmenite K <sub>sm</sub> Apatite K <sub>sm</sub>	Apatite $K_{sm}$	Biotite K <sub>sm</sub>
High K <sub>sm</sub>	1				ı	1	
$\mathbb{R}\mathbf{b}^2$	0.34	0.74	0.05	0.045	0.001	0.4	9.6
$Nb^3$	0.88	0.16	0.73	0.15	65.6	0.001	9.5
$\mathrm{Sr}^4$	13.1	22.1	0.17	0.001	99.0	2.4	7.2
$\mathrm{Ba}^5$	19.55	44	35	0.001	0.001	0.001	7
Low K <sub>sm</sub> <sup>1</sup>							
$Rb^2$	0.011	0.11	0.013	0.043	0.001	0.001	С
$Nb^3$	0.07	0.01	0.31	0.001	6.58	0.004	4
$\mathrm{Sr}^4$	4.04	2	0.17	0.093	0.17	2.1	0.12
$Ba^5$	_		0.063	0.001	0.001	0.001	3.7

<sup>1</sup> High K<sub>sm</sub> indicates values were among the highest listed in the GERM database; low K<sub>sm</sub> indicates values are among the lowest. K<sub>sm</sub> for quartz were not reported in the GERM database, so all were set to 0.001. <sup>2</sup> Rb mineral-melt partition coefficient references: Mahood and Hildreth, 1983; Mahood and Stimac, 1990; Ewart and Griffin, 1994; Stix and Gordon, 1994; Streck and Grunder,

Nb mineral-melt partition coefficient references: Nash and Crecraft, 1985; Bea and others, 1994; Ewart and Griffin, 1994; Horn and others, 1994; Klemme, 2003. 1997; Klemme and Dalpe, 2003.

<sup>4</sup> Sr mineral-melt partition coefficient references: Philpotts and Schnetzler, 1970; Watson and Green, 1981; Stix and Gordon, 1990; Ewart and Griffin, 1994; Streck and Grunder, 1997; Klemme and others, 2006.

<sup>5</sup> Ba mineral-melt partition coefficient references: Mahood and Hildreth, 1983; Ewart and Griffin, 1994; Stix and Gorton, 1990; Streck and Grunder, 1997.

TABLE 1B

	Range o	f Bulk Partition C	oefficients Used in	n Normalized Trac	Range of Bulk Partition Coefficients Used in Normalized Trace Element Calculations	$nS^{\circ}$
Element	Dry 0.1 GPa Isobaric	Wet 0.1 GPa Isobaric	Dry 0.3 GPa Isobaric	Wet 0.3 GPa Isobaric	Dry isentropic: 0.3 to 0.05 GPa <sup>7</sup>	Wet isentropic: 0.3 to 0.1 GPa <sup>7</sup>
High K <sub>sm</sub> <sup>1</sup>						
Rb	0.34-0.31	0.30-0.40	0.34-0.48	0.30-0.52	0.23-0.26	0.84 - 0.40
NP	0.88-0.65	0.79-0.49	0.88-0.69	0.81-0.58	0.62-0.69	0.83-0.49
Sr	13.1-10.5	11.5-12.4	13.1-10.6	11.2-12.0	8.77-9.84	10.2-12.5
Ba	19.6-18.6	17.2-24.0	19.6-18.3	19.1-22.1	14.4-16.7	17.7-24.0
Low $\mathbf{K}_{sm}^{-1}$						
Rb	0.01-0.03	0.02-0.05	0.01-0.10	0.01-0.11		
Nb	0.07-0.06	0.06-0.05	0.01-0.10	0.08-0.09		
Sr	4.04-2.19	3.56-1.75	4.04-2.16	3.46-1.77		
Ba	1.00-0.65	0.09-0.65	1.00-0.68	89.0-98.0		

<sup>1</sup> High K<sub>sm</sub> indicates values were among the highest listed in the GERM database; low K<sub>sm</sub> indicates values are among the lowest. K<sub>sm</sub> for quartz were not reported in the GERM database, so all were set to 0.001.

<sup>6</sup> Range represents from 100% melt to near-solidus.

<sup>7</sup> Range represents from 0.3 GPa, 50% partial melt (unlocked state) to 0.05 GPa for dry case and 0.1 GPa for wet case.

Oxide	Rhyolite (dry)	Rhyolite (wet)	Basalt
SiO <sub>2</sub> *	74.02	71.49	44.83
$TiO_2$	0.31	0.30	2.57
$Al_3O_2$	13.1	12.66	14.43
$Fe_2O_3$	0.34	0.44	2.21
FeO	1.63	1.48	10.89
MgO	0.31	0.30	7.29
CaO	1.21	1.17	9.56
$Na_2O$	3.28	3.17	2.42
$K_2O$	5.26	5.07	2.57
$P_2O_5$	0.04	0.39	0.55
$H_2O$	0.5	3.89	2.68

Table 2

Major Oxide Compositions of Rhyolite (M) Magma and Basalt (R) Magma

which is nearly saturated at 0.1 GPa. To compare the effects of pressure, wet and dry models were calculated at 0.1 and 0.3 GPa, corresponding roughly to depths of 3 km and 10 km, respectively. Simulations were run in equilibrium mode, using a 2 °C temperature increment, and  $fO_2$  for all runs was set along the QFM buffer. Table 2 summarizes the whole-rock major element compositions of the recharge basalt (**R** magma) and the rhyolite (dry and wet) (**M** magmas).

Starting from the rhyolite's near-solidus condition, where the system has  $\sim 2-3\%$ melt + < 0.5 wt. % fluid phase for the dry case, and  $\sim 2-3\%$  melt with  $\sim 3-4$  wt. % fluid phase for the wet case, for both pressures, the state of the magmatic system was assessed at  $\sim 10$  percent intervals to the **M** magma liquidus ( $\sim 10\%$  melt, 20% melt, *et cetera*). We define the steps to unlocking as those that produce partial melt up to  $\sim$ 50 percent in the rhyolitic mush. The enthalpy required to produce partial melt was calculated by subtracting the total enthalpy of the melt+solid+fluid rhyolitic system at a specific percent of partial melting and that of the near-solidus rhyolite. For example, the enthalpy difference between the dry rhyolitic system (0.1 GPa) at near-solidus conditions ( $\sim$ 3% melt) and  $\sim$ 10 percent melt is 17.6 kJ/kg. Available enthalpy comes from basalt cooling and crystallizing from its liquidus (1148 °C at 0.1 GPa) to a temperature that is in thermal equilibrium (±2 °C) with the rhyolite at a particular percent melt. For example, for the dry 0.1 GPa case at  $\sim$ 10 percent partial melt, the rhyolite temperature is ~745 °C, so the enthalpy available from the basalt is the difference between system enthalpy at its liquidus temperature and that at  $\sim$ 745 °C. Based on the required (for the rhyolite, 17.6 kJ/kg) vs. available (from the basalt, 910.3 k[/kg) enthalpy, a mass ratio of basalt (recharge) to rhyolite (silicic mush) is calculated ( $\sim 0.02$  for the example case), assuming 100 percent enthalpy transfer. A thermal efficiency factor for heat transfer from **R** to **M** may be incorporated into the analysis. For example, if half of the available heat from Ris is used to unlock M, then the effective mass ratio of **R** to **M** for unlocking would double to attain the same final state. For each step of partial melting for the four cases, the phase equilibria model also provides the relative masses of minerals, H<sub>9</sub>O fluid phase, and melt, as well as the compositions of minerals and melt. The phase equilibria, compositions, and temperatures of M at its near-solidus conditions, as well as the mass, thermal, major and trace element and mineralogical characteristics of these four systems as they undergo partial melting to unlocking are reported below.

<sup>\*</sup>All concentrations in wt. %.  $\rm Fe_2O_3$  and FeO calculated in Rhyolite-MELTS (Gualda and others, 2012) at 0.1 GPa and QFM.

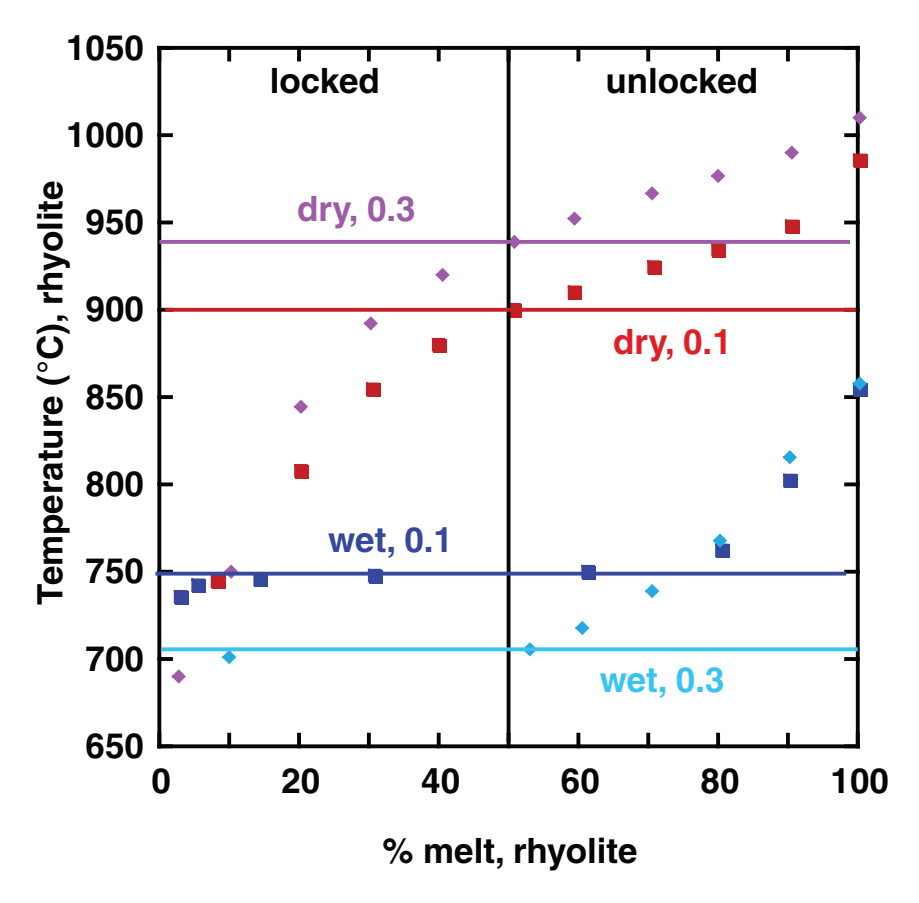


Fig. 2. Percent rhyolite melt, modeled as equilibrium melting from near solidus conditions to 100% melt versus temperature (°C) for four isobaric cases: wet (blue) and dry (red) 0.1 GPa and wet (turquoise) and dry (pink) 0.3 GPa. Magma mingling is treated as an isenthalpic process in all cases. 50% melt-50% crystals is defined as unlocked. The enthalpy required to partially melt from near-solidus conditions to the percent melt indicated (for example,  $\sim 10\%$ ,  $\sim 20\%$ ) is determined by Rhyolite-MELTS (Gualda and others, 2012), and assumes rhyolite mush and recharge basalt achieve thermal equilibrium subject to isenthalpic and isobaric equilibration at percent melt shown. Horizontal lines are guides that show y-axis value at unlocked state (50% melt). See text for additional description of conditions of unlocking. The same conditions of unlocking apply to all subsequent diagrams unless otherwise noted. Wet and dry cases show very different changes in temperature between the near-solidus and unlocked states.

#### Rhyolitic System at Near-Solidus Conditions

At its near solidus condition, the 0.1 GPa rhyolite crystalline assemblage (dry and wet) includes plagioclase, alkali feldspar, quartz, orthopyroxene, spinel, ilmenite, apatite, and  $\rm H_2O$  fluid phase; plagioclase, alkali feldspar, and quartz dominate the assemblages of all four cases. The near-solidus temperature for both the wet and dry cases is  $\sim\!737\,^{\circ}\rm C$  (fig. 2). For the 0.3 GPa cases, the phase assemblage is similar with the exceptions that apatite and orthopyroxene are not present but biotite (0.3 GPa case only) is. The near-solidus temperatures for these cases are  $\sim\!692\,^{\circ}\rm C$ . The SiO $_2$  concentration of the small proportion of melt for all the near-solidus cases is between  $\sim\!69.5$  and 73.5 weight percent.

Differences in the abundance of near-solidus phases (Appendix A, fig. 3) reflect different initial (liquidus) H<sub>2</sub>O concentrations. In both wet cases, alkali feldspar is the

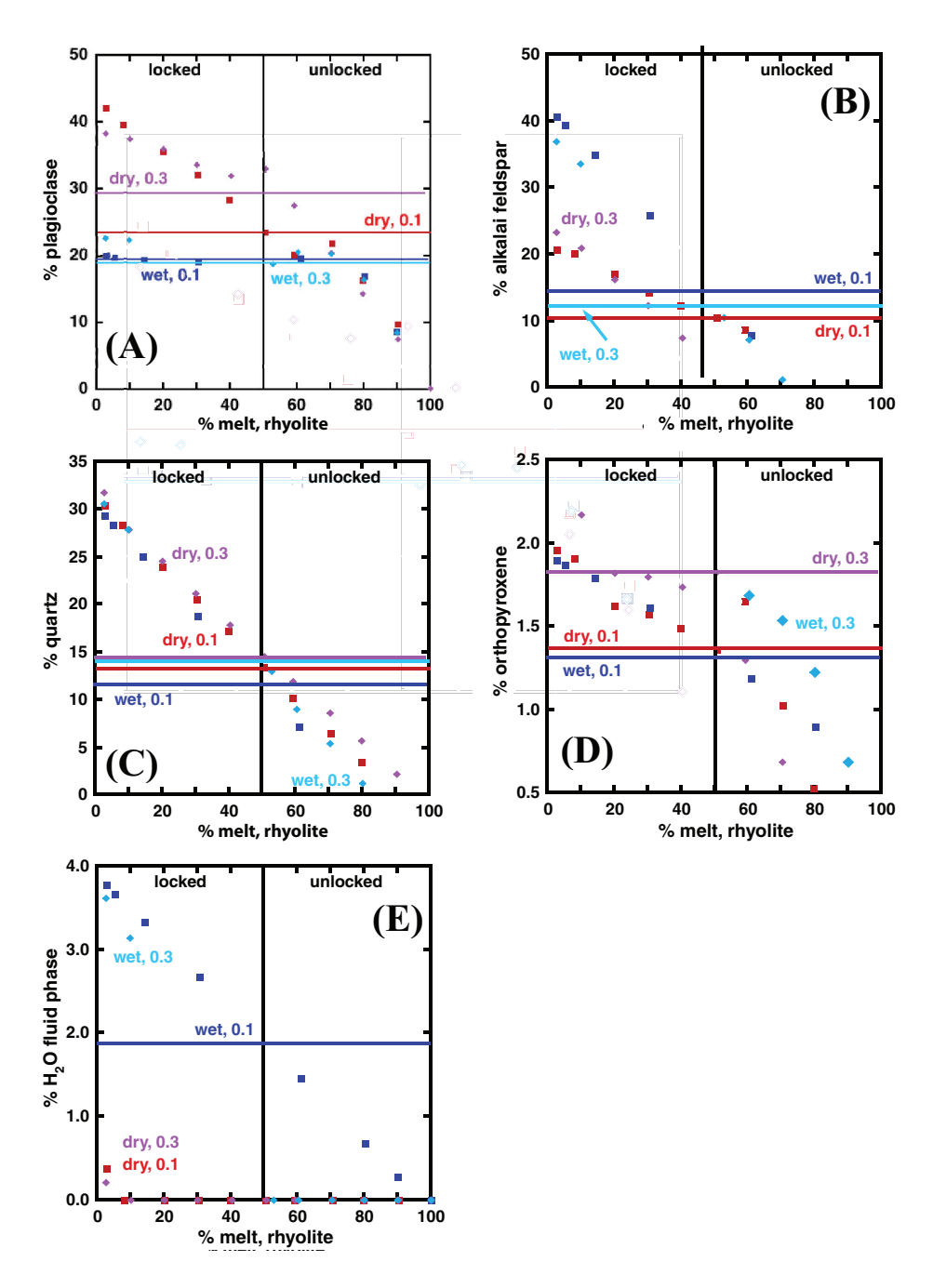


Fig. 3. Percent rhyolite melt versus percent mineral phase in magma system, which includes melt + solids+ fluid phase, for four cases. (A) Plagioclase, (B) alkali feldspar, (C) quartz, (D) orthopyroxene, (E)  $\rm H_2O$  fluid phase. Differences in abundances of plagioclase and alkali feldspar are observed between wet and dry cases. Unlocking is dominated by a decrease in mineral proportion, but several cases show some crystal growth during unlocking. See text for discussion. Colors are the same as figure 2.

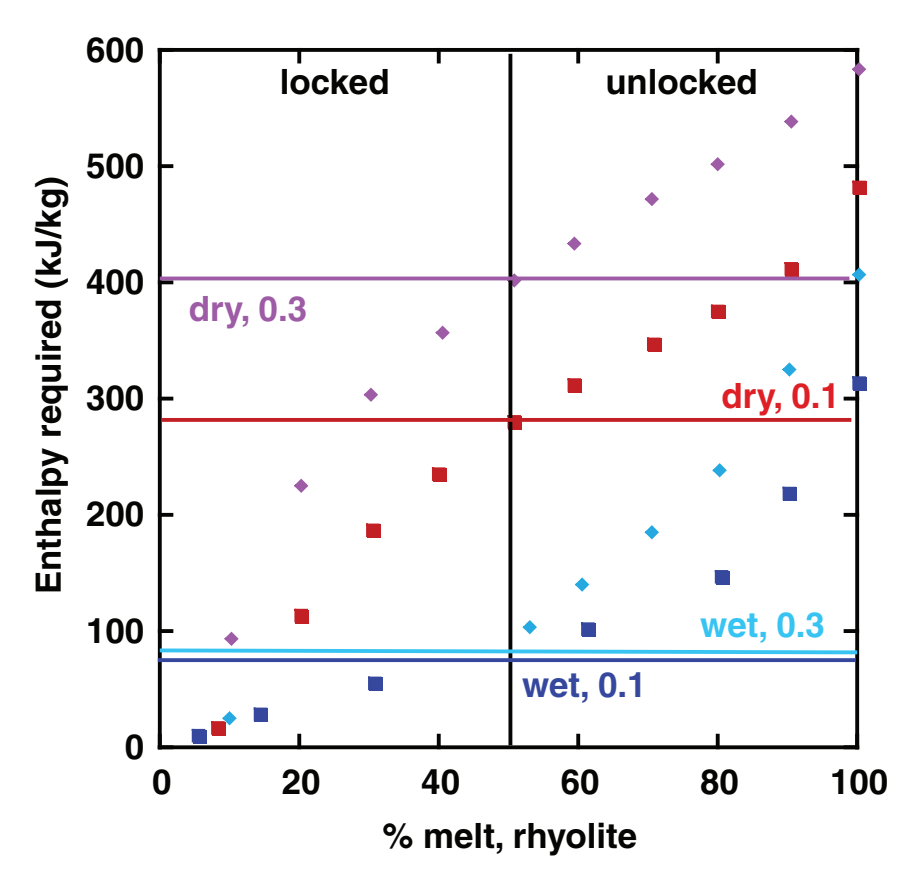


Fig. 4. Percent rhyolite melt versus enthalpy required to unlock from near-solidus to % melt shown. Enthalpy is expressed in kJ/kg of silicic magma. Note that dry rhyolite systems require more enthalpy to unlock than the wet systems. Colors are the same as figure 2.

dominant feldspar phase, whereas for the dry systems, plagioclase is the dominant feldspar. The abundances of quartz among the four cases are similar, and orthopyroxene is similar for the two 0.1 GPa cases. For the 0.3 GPa cases, it is not a part of the near-solidus assemblage. Fluid concentrations are also different, with the dry cases containing <0.5 percent  $H_2O$ , and the wet cases containing between 3.6 and 3.8 weight percent at near-solidus conditions.

Constraints on a Rhyolitic System During Equilibrium Partial Melting to Unlocking

Starting with the near-solidus systems described above, the addition of enthalpy from the basalt (evaluated at thermal equilibrium with rhyolite) causes partial melting in the mush. Appendix A summarizes enthalpy, temperature, mass ratio, and mineral characteristics of basalt and rhyolite at each "step" during partial melting, and also provides the major element compositions of rhyolitic melt at each step as the fraction of melt in **M** increases during defrostive unlocking.

For the four cases, the enthalpy requirements (kJ/kg of rhyolite melt+solids+fluid) for melting from near-solidus conditions to a particular percent partial melting are different (fig. 4); in general, the dry 0.3 GPa case is the most energy-intensive, whereas the wet 0.1 GPa is the least. This is simply related to the fact that at fixed pressure, the

melt fraction present depends on enthalpy and M composition such that 'wet' magma partially melts more easily than 'dry' magma. That is, the enthalpy requirements for unlocking the dry systems are  $\sim 3$  to 4 times more than those for the wet systems. The H<sub>2</sub>O content of **M** rhyolite plays a dramatic role in reducing the heat requirement for unlocking, in a first-order manner. It is important to emphasize that no mass is exchanged between **R** and **M** during the unlocking calculations presented here; this is a case of magma mingling, not magma hybridization. That is, each sub-system (M and **R**, respectively) is closed with respect to mass exchange but open with respect to heat exchange. The slopes of enthalpy versus percent rhyolite melt are different as well; compared to the dry cases, the wetter ones have shallower slopes from near-solidus to  $\sim$ 60 percent partial melt. The 0.3 GPa dry case has the steepest slope of the four cases, consistent with this case requiring the greatest input of enthalpy to achieve a particular percent partial melting. The liquidus temperatures ( $T_{liq}$ ) of the dry cases ( $\sim 1000$  °C) are higher than those of the wet cases (~850 °C) (fig. 2). It is emphasized that in the wet cases, the temperature of M changes very little during unlocking as the melt fraction increases substantially. Thus, geothermometers are not especially sensitive to the wet unlocking process. On the other hand, the viscosity of the magmatic mixture (solid+melt+fluid) is quite sensitive to the melt fraction and hence changes dramatically as the critical unlocking melt fraction is approached. Similarly, trace element concentrations in crystals will vary under isothermal-isobaric conditions as the fraction of melt in M increases during unlocking. If trace element equilibration is not attained then the partition coefficient as well as diffusivity of each trace element will control its concentration profile in the crystal.

The enthalpy provided by the **R** basalt (Appendix A) as it cools and crystallizes from its liquidus ( $\sim$ 1148 °C at 0.1 GPa;  $\sim$ 1160 °C at 0.3 GPa; fig. 5) provides the energy for unlocking. Because typically, under constraints of thermal equilibrium, cooling and crystallization of basalt produces more enthalpy per kg than is required to heat up and partially melt 1 kg of rhyolite, the mass ratios of basalt to rhyolite are generally less than 1 assuming (1) that all of the heat available from  $\mathbf{R}$  goes into unlocking  $\mathbf{M}$  and is not dissipated externally, and (2) the required and available enthalpies are calculated for rhyolite and basalt that come to the same final temperature (that is, achieve thermal equilibrium). The impact of imperfect energy transfer could be accommodated through use of a heat transfer efficiency factor. For example, if half of the available heat from **R** goes into warming up wallrock rather than unlocking **M**, then twice as much **R** would be needed to mobilize **M**. It is difficult to know the amount of 'waste heat' without solving an accurate heat transfer model in three-dimensions with many thermophysical parameters that, unfortunately, are often poorly known generally. Our model does provide a lower limit on the mass of R needed to unlock M. Note that the enthalpy available from  $\mathbf{R}$  at any temperature, not just at thermal equilibrium with **M** magma, can be evaluated in Rhyolite-MELTS. Thus, different scenarios where these assumptions are relaxed can be explored. In all the results presented here, the criterion of thermal equilibration between M and R was adopted and all available R heat goes into M.

For the four cases, the mass ratios of basalt recharge magma to rhyolite mush  $(\Re \equiv M_R/M_M \text{ fig. 6})$  range from  $\sim 0.1$  to 0.7 at the unlocked state of M. These are minimal mass ratios for the reasons stated above. Consistent with the enthalpy requirements described above, the wet cases require relatively low mass ratios  $M_R/M_M$  ( $\sim 0.1-0.15$ ), whereas the dry cases require higher ones (0.4-0.7). Note that for complete melting, that is, to generate essentially aphyric silicic melt, the dry cases require  $M_R/M_M > 1$ . This constraint is tied to the assumption of thermal equilibrium; the basalt can only cool and crystallize to the  $T_{liq}$  of the rhyolite ( $\sim 1000$  °C), and thus because the total amount of enthalpy generated is comparatively modest, the  $M_R/M_M$ 

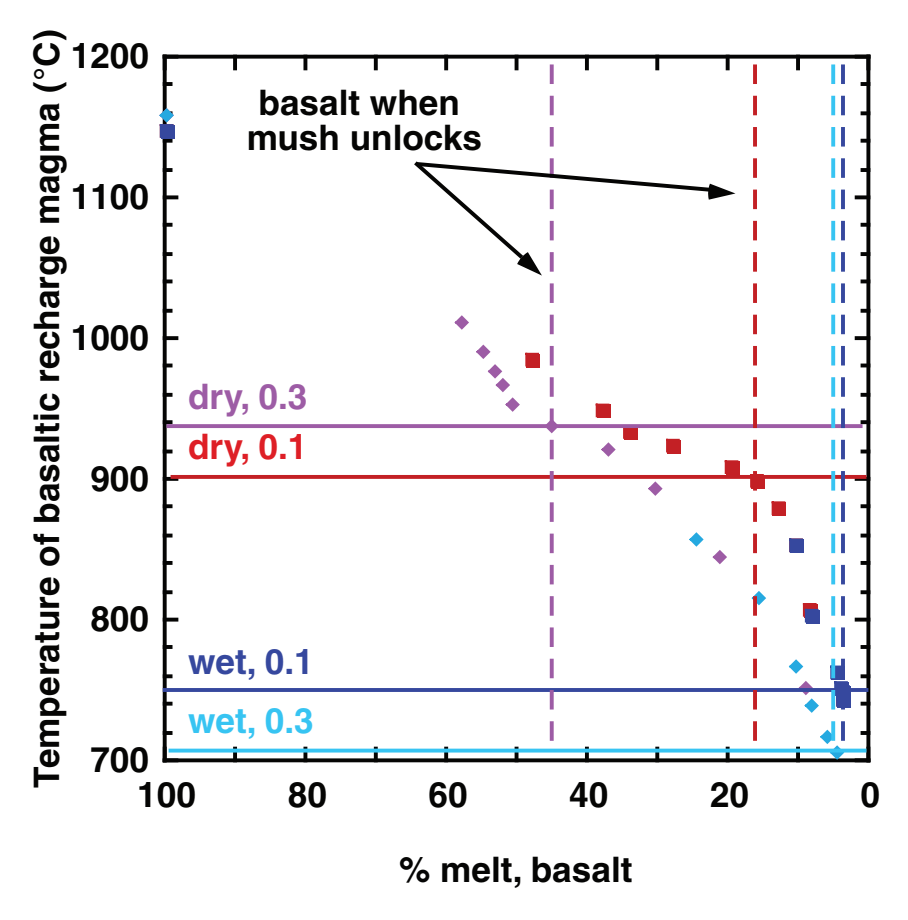


Fig. 5. Percent recharge basalt melt versus basalt temperature (°C). Horizontal lines show temperature of basalt and rhyolite in thermal equilibrium at 50% rhyolite melt. Vertical lines illustrate % melt of recharge basalt when silicic magma is unlocked. Wet cases require almost complete basalt crystallization whereas dry cases require less crystallization. Colors are the same as figure 2.

requirements are larger than cases where the basalt can cool to lower temperatures (for example,  $T_{liq}$  of wet rhyolite ~850 °C). Clearly, the lower  $T_{liq}$  of the wet cases means that the basalt cools and crystallizes more, thus producing more enthalpy.

Like the enthalpy and mass requirements, the temperatures of the rhyolitic  $\mathbf{M}$  systems as partial melting occurs are also different (fig. 2). In the case of a dry rhyolitic mush, temperature increases during partial melting fairly dramatically; the temperature change from near solidus to the unlocked state is  $\sim 165~(0.1~\text{GPa})$  and 250 °C (0.3 GPa). In contrast, the wet systems show only modest temperature increases ( $\sim 15~\text{°C}$ ) from near solidus conditions to the unlocked state, consistent with pseudo-invariant melting behavior (Fowler and others, 2007). The proclivity of magma to approach invariant point-like behavior is a strong function of its dissolved  $H_2O$  content and its anhydrous bulk composition. Because the energy requirement for unlocking scales with  $\mathbf{M}$  magma water content, the unlocking probability correlates with the volatile content of  $\mathbf{M}$  magma. Volatile—saturated silicic magma that is simultaneously saturated with quartz, plagioclase and alkali feldspar is, from an energy point of view, relatively easy to unlock. The heat added to silicic mush from  $\mathbf{R}$  magma goes to increasing the

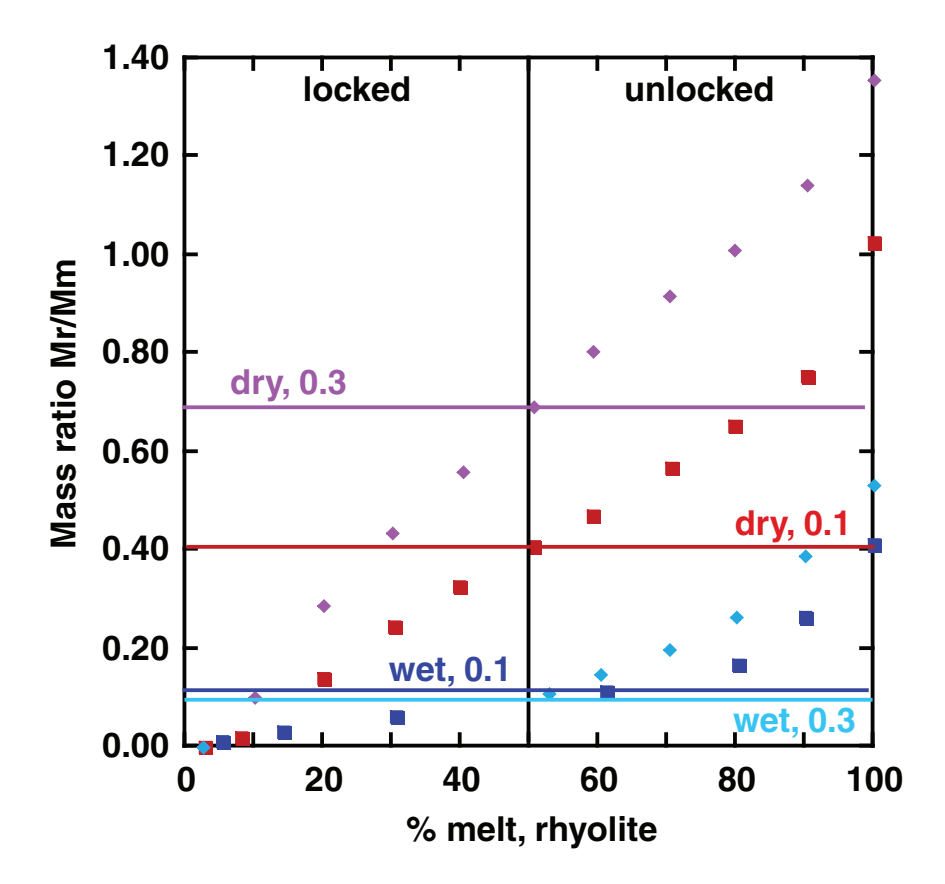


Fig. 6. Percent rhyolite melt versus  $M_R/M_M$  mass ratio for the four cases. Dry cases require larger masses of recharge magma to unlock. Colors are the same as figure 2.

melt fraction (latent effect) rather than being 'wasted' by raising the temperature of the silicic magma when M magma is at or near an invariant point. This is a purely thermodynamic phenomena related to the low thermodynamic variance of the silicic system. The critical issue is the unlocking timescale, a heat transport problem, and not the energy requirement. Although the effects of  $H_2O$  on the explosivity of magma upon decompression are well known, the phenomenon noted here, while related, is distinct.

As noted above, the near solidus assemblage for all cases is dominated by plagioclase, alkali feldspar, and quartz. H<sub>2</sub>O fluid phase is also present in all cases. Minor phases include orthopyroxene, spinel, ilmenite, apatite and biotite. We focus this discussion on the most abundant phases, and acknowledge that accessory phases such as allanite and zircon, which are not modeled in Rhyolite-MELTS, can also provide critical information about partial melting and unlocking. In all cases, quartz is consumed during unlocking (fig. 3C). New growth of quartz (that is, rims) is therefore not an outcome of the unlocking models presented here. During perfect equilibrium melting, quartz will record the rising **M** magma temperature (if temperature increases) associated with unlocking, and this record might be deciphered using Ti in quartz geothermometry. However, because unlocking is unlikely to be a perfect equilibrium process, the nature of this signal would be modulated by the interplay of the timescales for reactive interface dissolution kinetics, diffusion of Ti in the melt, and the local

increase in the melt fraction associated with unlocking. If quartz bulk dissolution rates were large compared to melt-quartz interface kinetics, for example, Ti-zoning evidence could be muted or even absent. Even if a record is preserved, observed patterns might not simply translate to estimates of unlocking times and may constrain interface kinetics instead. More analysis, beyond the scope of this study, is required to understand the possibilities more fully.

Distinctions in the abundances of plagioclase and alkali feldspar highlight differences in the wet and dry systems (figs. 3A and 3B). Alkali feldspar is more abundant in the wet cases (both pressures) than the dry when partial melt is  $\leq 50$  percent. In all cases, alkali feldspar decreases in abundance as partial melting progresses, and therefore, like quartz, there is no evidence of crystallization of alkali feldspar on the pathway to unlocking. In contrast, plagioclase does not show simple, systematic trends during unlocking. It is more abundant in the dry cases and generally decreases in abundance as mush partially melts. An exception is between  $\sim$ 40 and 50 percent melt in the dry 0.3 GPa case; its abundance increases slightly. (Similar small increases in plagioclase abundance are seen between  $\sim$ 60 and 70 percent melt in the dry 0.1 and wet 0.3 GPa cases). Although the increases are very small, the critical point is that modest new growth may occur, a record of which might be preserved in plagioclase rims in volcanic rocks. In the wet cases, on the path to unlocking, plagioclase abundances barely change (that is, decrease less than 4%). For the wet 0.1 GPa case, orthopyroxene abundance decreases systematically. For the dry cases, the trajectories show modest increases in abundance between  $\sim$ 40 and 60 percent melt. Therefore, in these cases, new (modest) growth of orthopyroxene is predicted. Orthopyroxene is not stable in the wet 0.3 GPa case until  $\sim 60$  percent melt.

We emphasize that whether a phase suffers net loss (resorption), net growth, or reactive dissolution/precipitation with mass exchange between former crystal and melt depends on the specifics of the phase equilibria. To make matters even more complicated, if interface kinetics, crystal growth and dissolution rates, and differential diffusion of major and trace elements are considered, blanket statements cannot be made. One must study the phase equilibria in detail given the specific conditions of bulk composition, temperature, pressure, and redox state in addition to nonequilibrium effects. Specifically, the timescales associated with nonequilibrium processes may be highly disparate and that can obfuscate the extraction of an unlocking time from zoning trends in specific phases.

Major element changes in the liquid during partial melting are presented in Appendix A. Compared to the near-solidus melt compositions, for all cases, as progressive partial melting occurs to the state of unlocking, SiO<sub>2</sub> and Al<sub>2</sub>O<sub>3</sub> concentrations increase relatively (in the first 10-20% melting) and then the slopes of the concentration vs. % rhyolite melt trends approach 0. In the first 10 to 20 percent melting, P<sub>2</sub>O<sub>5</sub> and CaO concentrations decrease sharply and at higher degrees of melting, change little. MgO behaves differently for the four cases; it generally increases for the 0.1 GPa cases (although non-monotonically), whereas for the 0.3 GPa cases, concentrations do not change significantly until ~60 percent partial melt. TiO<sub>2</sub> and H<sub>2</sub>O (component) behave differently based on pressure as well. In the 0.1 GPa cases,  $TiO_2$  increases to near its maximum concentration at  $\sim 50$  percent melt, and then decreases at higher degrees of melt, whereas H<sub>2</sub>O systematically decreases. For the wet 0.3 GPa case, TiO<sub>2</sub> concentrations do not change appreciably until after the system reaches ~50 percent melt. H<sub>2</sub>O changes are also modest until ~50 percent melting, whereas at higher degrees of melt, its concentration systematically decreases. In the dry 0.3 GPa case, concentrations of TiO<sub>2</sub> and H<sub>2</sub>O change very little from near solidus to liquidus temperatures. For the 0.1 GPa and the dry 0.3 GPa cases, K<sub>2</sub>O initially increases and then decreases, achieving values that are slightly higher than the

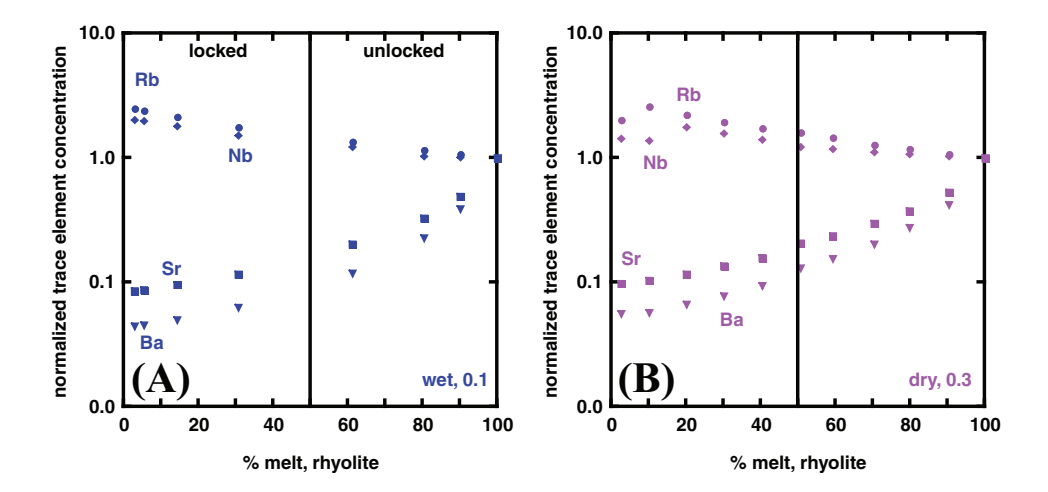


Fig. 7. Percent rhyolite melt versus normalized melt Sr, Ba, Rb and Nb concentrations, assuming chemical equilibrium.  $K_{\rm sm}$  for each mineral, element chosen from among the highest in the GERM database. See table 1A for mineral-melt partition coefficients and references. Trends for elements are very similar among the four cases so only the wet 0.1 and dry 0.3 GPa cases are shown.  $K_{\rm sf}=1000$ . See text for discussion. Colors are the same as figure 2.

near-solidus melts.  $Na_2O$  is the opposite; it initially decreases and then increases. For both of these elements, the wet 0.3 GPa case lacks the distinct concavity that the other cases have; after the initial increase or decrease, the concentrations do not change significantly to the unlocking point.

Trace element changes were explored for each of the four thermodynamic cases using elements that span a range of behaviors: Sr, Rb, Nb, and Ba. (We excluded elements such as the REE and Zr from this analysis because Rhyolite-MELTS does not handle zircon and allanite). In this section, we illustrate how these trace elements change concentration in the M melt during unlocking, explore trace element concentration variations as a function of different K<sub>sm</sub>, and examine the implications of element partitioning if a fluid phase is present. Table 1 summarizes K<sub>sm</sub> for each phase, element (with relevant references), and range of bulk  $K_{sm}$  for each model. For the cases shown in figure 7,  $K_{sm}$  were chosen from among the highest values listed in the GERM database. For comparison, we also discuss trace element behavior when  $K_{\rm sm}$  are among the lowest. (For both sets of  $K_{sm}$ , because we focus on the general behavior of the elements during partial melting, mineral-melt partition coefficients were not varied based on their sensitivity to composition or temperature).  $K_{sf}$  are set at 1000 and 0.001 to bracket the behavior of fluid insoluble and fluid soluble elements, respectively. For this discussion, trace element results are normalized to the bulk concentration of M to obviate the need to define initial concentrations, which can vary widely in rhyolitic magmas.

Because the trace element analysis yielded very similar results for all four cases, only 2 (wet 0.1 GPa and dry 0.3 GPa) are presented in figure 7 (where  $K_{\rm sf}$  are set to 1000). In all cases, Sr and Ba act compatibly (bulk  $K_{\rm sm} > 1$ ), whereas Rb and Nb behave incompatibly. Ba is the most compatible element in all cases, and normalized concentrations in melt increase as partial melting progresses toward unlocking. The bulk  $K_{\rm sm}$  is dominated by the  $K_{\rm sm}$  of alkali feldspar. Sr also increases in concentration in the melt during unlocking, and its behavior is influenced by  $K_{\rm sm}$  of both plagioclase and alkali feldspar. Nb and Rb behave fairly similarly, although at small degrees of partial melt

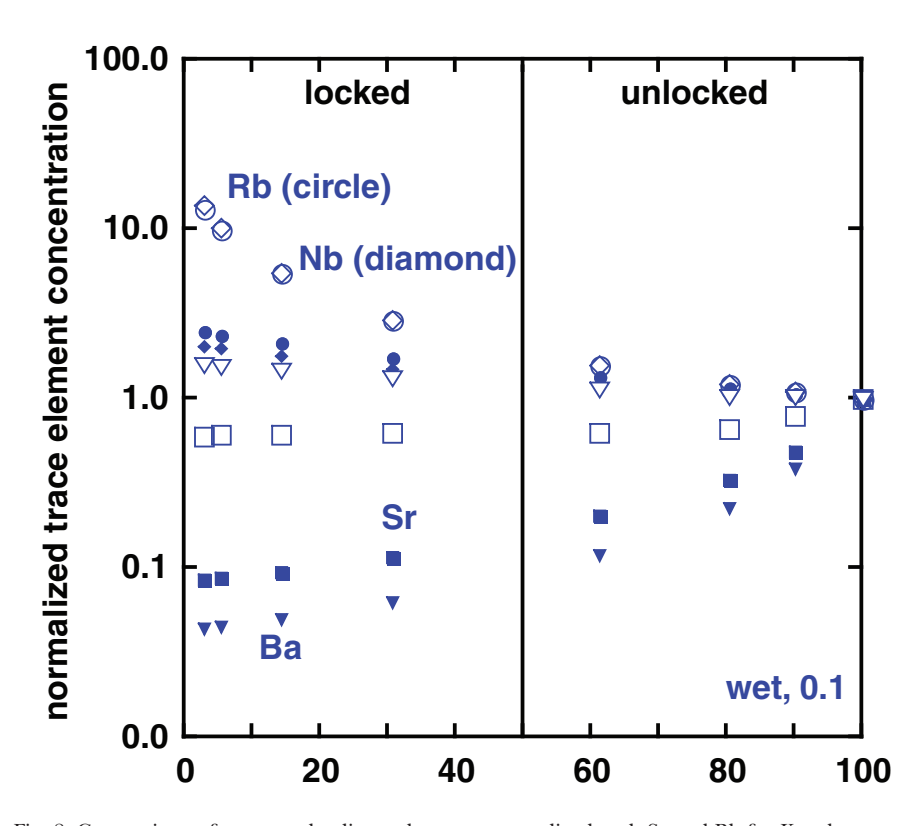


Fig. 8. Comparison of percent rhyolite melt versus normalized melt Sr and Rb for  $K_{\rm sm}$  that are among the highest (closed symbols) and among the lowest (open symbols).  $K_{\rm sf}=1000$ . Comparison illustrates trace element characteristics of melt and crystals (resorbed or newly grown) will vary depending on bulk  $K_{\rm sm}$ , assuming chemical equilibrium. A key difference is the behavior of Ba, which changes from bulk  $K_{\rm sm}>1$  (closed symbols) to <1 (open symbols). This difference is important because it illustrates that during unlocking, Ba concentration can increase in crystals (re-equilibrated during resorption or newly grown) or decrease. Knowledge of the phase equilibria and mineral-melt partition coefficients is important for diagnosing the difference between crystal characteristics in unlocking versus (for example) isentropic ascent. See text for additional discussion.

(that is, near solidus conditions), Nb is slightly less incompatible because of apparent compatibility in ilmenite; however, this effect is subtle since ilmenite is a minor phase. As partial melting progresses to unlocking (and beyond), Nb and Rb decrease in concentration in melt

In figure 8, behaviors of these four elements are compared by illustrating normalized concentration changes during partial melting for  $K_{\rm sm}$  that are among the highest (as discussed above) and the lowest found in the GERM database. Because all of the cases show similar behavior, we discuss only the wet 0.1 GPa case. Predictably, enrichments of Rb and Nb are higher at lower degrees of partial melting (that is, near-solidus conditions), but at unlocking, the differences between the "high" and "low"  $K_{\rm sm}$  cases are subtle. The Sr and Ba differences are more robust. While Sr remains compatible, the degree of depletion is less in the low  $K_{\rm sm}$  case compared to the high  $K_{\rm sm}$  case. Thus, the differences between the Sr concentrations in melt in the near-solidus state and at unlocking will be significantly smaller than for the high  $K_{\rm sm}$  case. That is, for the low case, the slope of normalized trace element concentration in M melt vs. the percent melt in M magma is very close to 1. Because the bulk  $K_{\rm sm}$  for Ba is  $\leq 1$  for the low  $K_{\rm sm}$  case, this element acts incompatibly, and thus the Ba melt

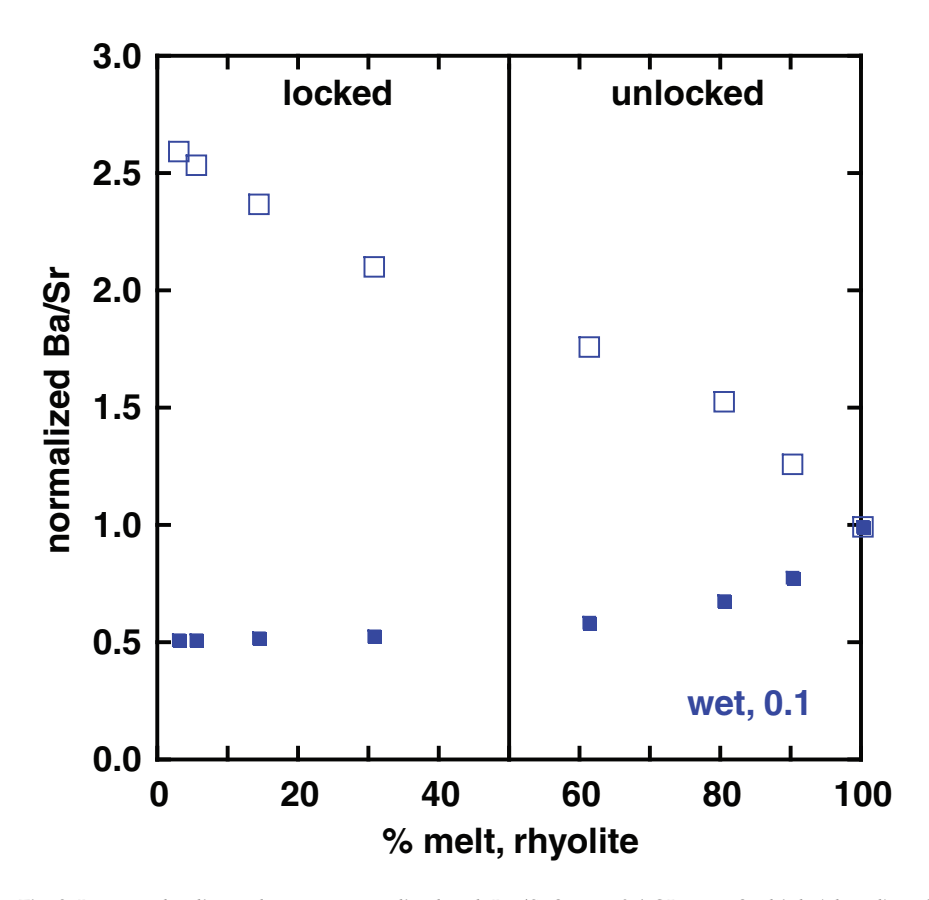


Fig. 9. Percent rhyolite melt versus normalized melt Ba/Sr for wet 0.1 GPa case for high (closed) and low (open) mineral melt partition coefficients. Note that during unlocking, depending on the behavior of Ba, the ratio can decrease or increase.

concentration decreases during partial melting, although the effect is subtle (slope close to 1). Ba/Sr changes slope (fig. 9), with the high  $K_{\rm sm}$  case showing an increase in Ba/Sr during partial melting, and the low showing a decrease.

One additional comparison highlights the necessity of understanding phase equilibria in order to accurately document processes and timescales of unlocking. Figure 10 compares the behavior of Sr and Rb for the wet 0.1 GPa case when an element is soluble ( $K_{\rm sf}=0.001$ ) vs. insoluble ( $K_{\rm sf}=1000$ ) in a  $H_2O$  fluid phase. The concentrations of both elements are (predictably) much lower in the  $K_{\rm sf}=0.001$  case because most of the element is partitioned into the fluid phase. Sr remains compatible, but its concentration in melt (and that available for partitioning into minerals) is much lower than in the  $K_{\rm sf}=1000$  case. Rb increases in concentration in the melt as partial melting progresses in the  $K_{\rm sf}=0.001$  case because of the partitioning into the fluid phase. This change is the opposite of the behavior of the  $K_{\rm sf}=1000$  case where Rb concentration will decrease as percent partial melt increases. The choice of 0.001 is intentionally extreme to illustrate the potential variability in trace element behavior during partial melting and unlocking.

In summary, as unlocking proceeds, melt concentrations decrease for incompatible elements but increase for compatible elements. For phases that experience crystal

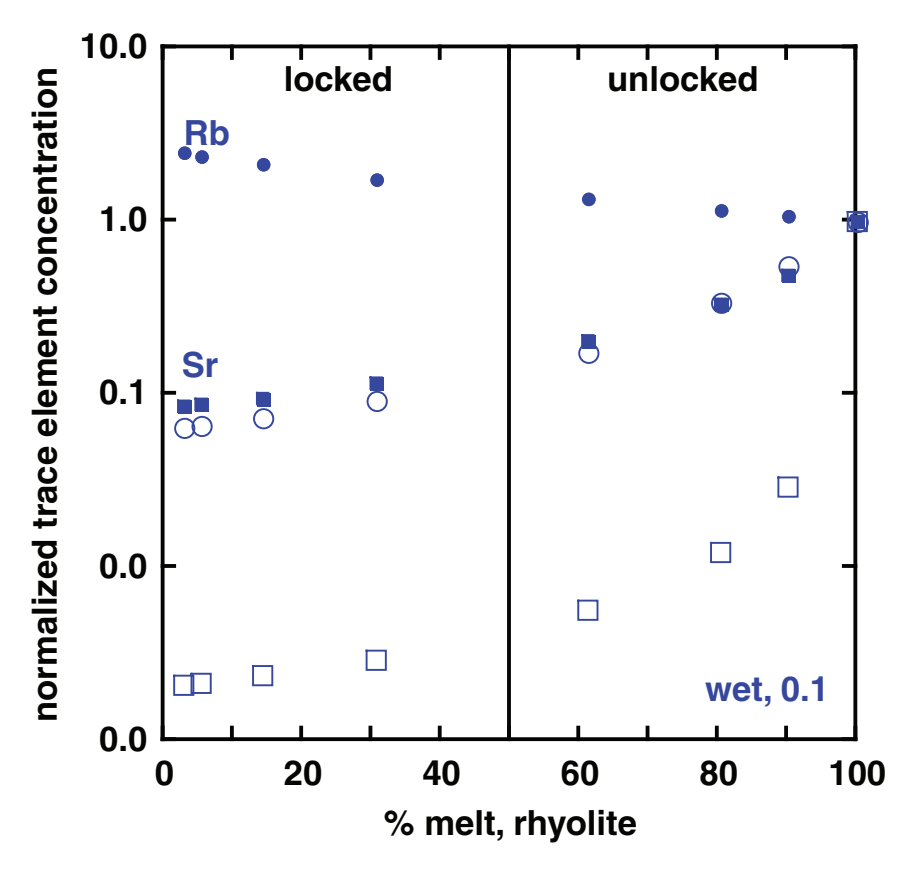


Fig. 10. Comparison of percent rhyolite melt versus normalized melt Sr and Rb for  $K_{\rm sf}=1000$  (closed symbols) and 0.001 (open symbols).  $K_{\rm sm}$  are those of figure 7. Comparison illustrates trace element characteristics of melt and crystals during unlocking will vary depending on whether elements are fluid soluble or not, and concentration of fluid phase.

growth or when re-equilibration successfully records the unlocking process in crystals (that is, interface kinetics favor re-equilibration of all or some part of the crystal with melt as it changes composition during unlocking) similar patterns may be preserved during unlocking. For example, rims may be enriched in compatible and depleted in incompatible elements compared to cores. In the presence of fluid, depending on the  $K_{\rm sp}$ , fluid soluble elements may be more enriched in rims than cores as unlocking progresses. Thus, the difference between fluid-present and fluid-absent behavior of typically incompatible, but fluid-soluble elements (for example, Rb), is potentially important for predicting rim characteristics during growth related to unlocking.

## Comparison of Unlocking by Equilibrium and Fractional Melting

Modeling unlocking as an equilibrium process represents one end-member of a span of possible behaviors. At the other extreme is perfect fractional melting. While melting (and crystallization) processes in magmas lie along a spectrum between these idealized extremes, equilibrium and fractional melting likely bracket the range of unlocking behaviors. We therefore compare equilibrium and fractional partial melting for one case (wet 0.1 GPa case) to highlight similarities and differences in mineral identities and abundances and elemental trends. In this comparison, all parameters

are identical except the style of melting. For these two melting styles, the relationships between percent melt, temperature, and mineral abundances are similar, when the percent melt for the fractional case is based on the cumulative amount of melt. Major element compositions of equilibrium vs. fractional melts are similar up to  $\sim$ 80 percent melt. While a full analysis of trace elements, including calculation of different bulk K<sub>sm</sub> as melting progresses and phase abundances change, is beyond the scope of this paper, figure 11 illustrates the normalized instantaneous and average melt trace element concentrations ( $C_m/C_m^o$  and  $\hat{C}_m/\hat{C}_m^o$ , respectively) for different bulk  $K_{sm}$  (0.1 – 10) for fractional melting. The instantaneous concentration represents the trace element concentration of each melt increment formed (and removed) during fractional melting, whereas the average represents the aggregate (average) of all increments along the melting path from the solidus. For more information about these and the relevant equations, see Spera and others, 2007. Results for average melt compositions  $(\hat{C}_m/\hat{C}_m^o)$  are considered more comparable to equilibrium melting, particularly for the phenomenon of unlocking, where aggregate melts are required to bring about the increase in the local fraction of melt in M needed for eruption. While the detailed trends differ, behaviors of compatible and incompatible elements are generally similar between equilibrium and fractional melting; for both processes, during unlocking, compatible elements concentrations of melt (and any associated crystals that form or re-equilibrate) increase, whereas incompatible element concentrations decrease. Therefore, given the similarities in elemental, temperature, and phase equilibria characteristics between the equilibrium and fractional melting cases, the analysis that we present below utilizes equilibrium melting results

## Magma Ascent After Unlocking

The unlocking cases described above were run isenthalpically and isobarically. Based on the phase equilibria results, there is no evidence of substantial increase in the abundance of one phase at the expense of another as unlocking occurs (fig. 3). And yet, numerous studies document rim growth on crystals apparently in response to unlocking prior to eruption. Additional phase equilibria calculations run under different conditions (for example, bulk composition of M magma, redox condition, pressure) may reveal examples where substantial growth of selective phases can occur even as mush undergoes partial melting to an unlocked state. This should be addressed in future studies. But the lack of significant new growth led us to consider other processes that might yield substantial new growth. One possibility is that crystal growth may be the result of decompression as magma ascends upwards. To simulate decompression and ascent of an unlocked magma, the dry and wet 0.3 GPa cases were modeled by first melting the systems under equilibrium conditions to  $\sim 50$  percent partial melt. Each magma (crystals+melt±fluid phase) then underwent isentropic decompression from 0.3 GPa towards the surface. Figures 12, 13 and 14 show the temperature, phase equilibria and Rb and Sr concentration consequences of this change. Ascent of the dry mush from 0.3 to 0.05 GPa increases the proportion of melt in the mush, and decreases the abundances of minerals. Temperature also decreases. Thus, no new growth is recorded among any of the minerals. Normalized Rb and Sr concentrations are very similar to the isobaric case. In contrast, as the wet magma ascends from 0.3 to 0.1 GPa, it decreases in melt abundance and increases modestly in temperature (due to latent heat of crystallization). Quartz and alkali feldspar increase in abundance (figs. 13C and 13B), whereas plagioclase abundance first increases and then decreases (fig. 13A). Orthopyroxene is not stable at 50 percent partial melt in the wet system, and only reappears as a stable phase at near solidus conditions (fig. 13D). Rb and Sr concentrations for this case are similar to those of the isobaric case at the same percent melt. We note that the decrease in melt abundance for this case may

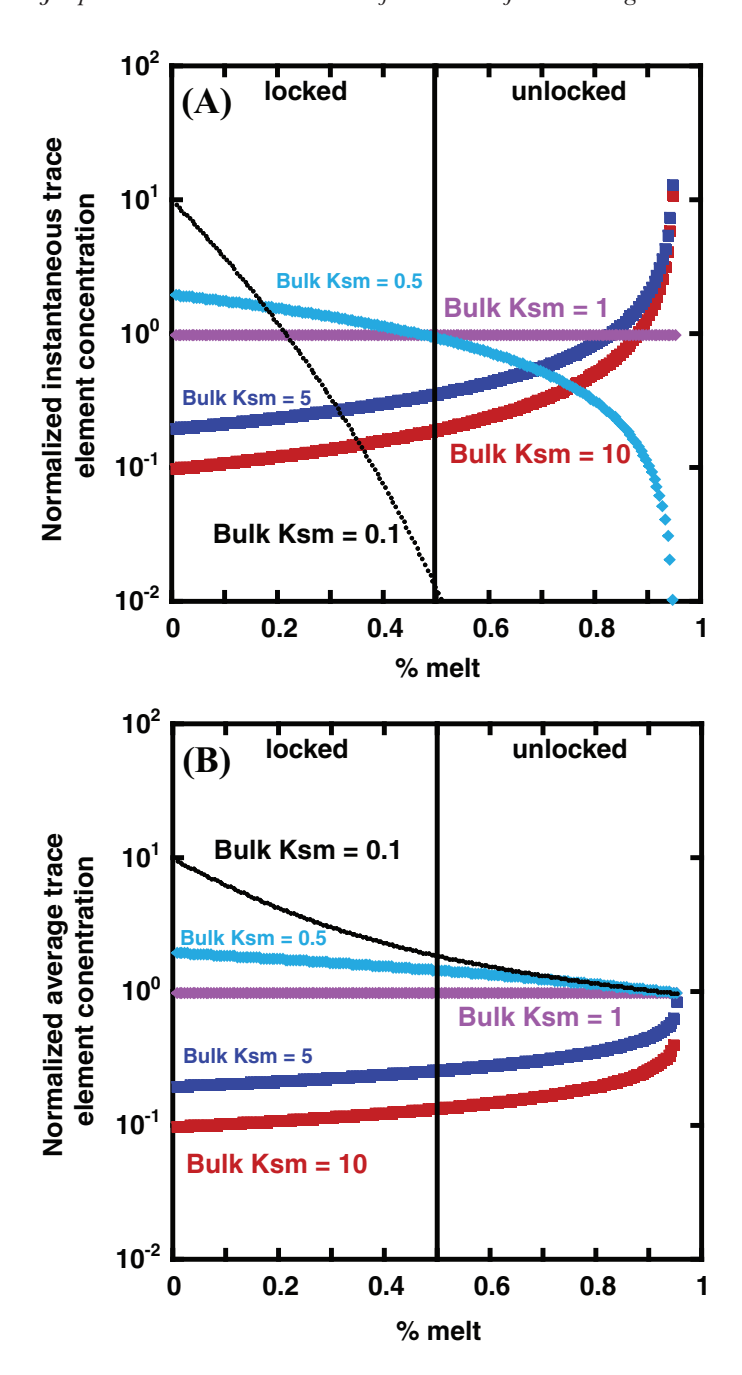


Fig. 11. Percent rhyolite melt versus normalized melt trace element concentrations for fractional crystallization. A range of bulk  $K_{\rm sm}$  is shown from 0.1 to 10. (A) Normalized instantaneous concentration; (B) normalized average concentration. Note that slopes for incompatible and compatible elements are similar to those calculated for the equilibrium cases. See text for further explanation.

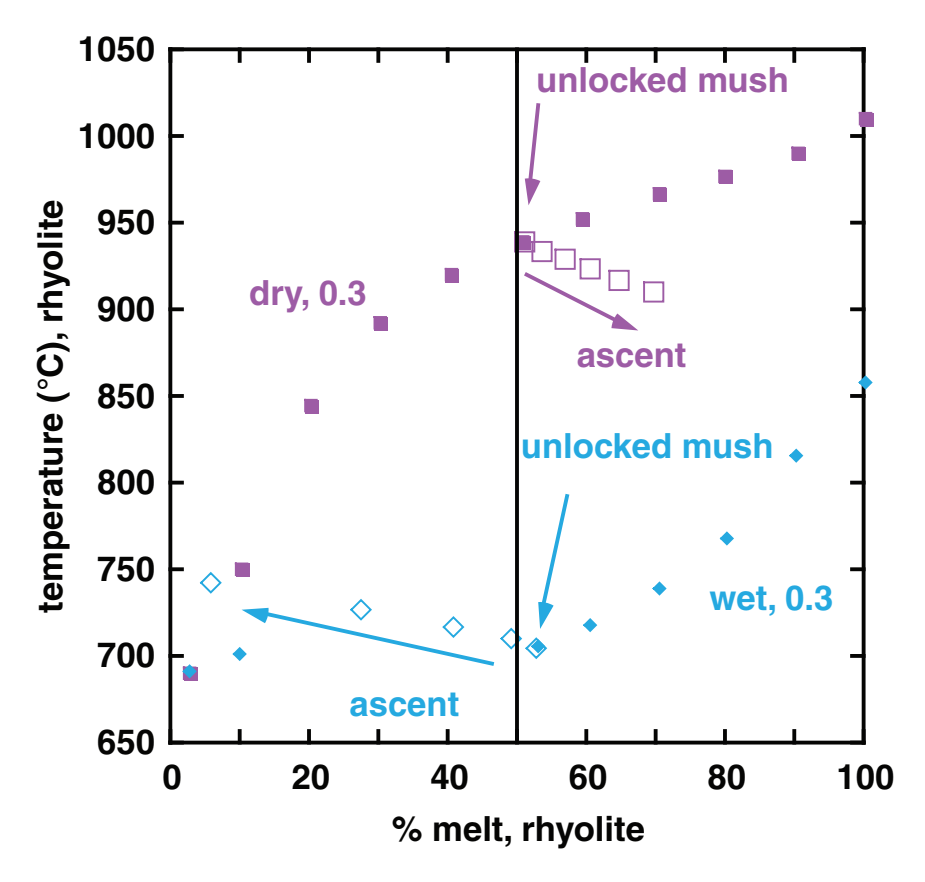


Fig. 12. Percent rhyolite melt versus rhyolite temperature ( $^{\circ}$ C) for wet and dry 0.3 GPa cases where solid symbols show unlocking. Open symbols represent isentropic ascent paths that initiate at 0.3 GPa and 50% melt and stop at 0.1 GPa (wet) and 0.05 GPa (dry). In the dry case, percent melt increases; in the wet case, crystal modal abundance increases. Colors same as figure 2.

preclude ascent as modeled. The analysis we present is a thermodynamic treatment intended to illustrate the consequences of ascent of this wet magma, including possible new crystal growth; addressing whether such ascent is realistic and will lead to eruption is beyond the scope of this paper. We also note that other processes, such as volatile loss, may also lead to crystallization. What is critical is that growth did not take place during the process of unlocking, but is a post-unlocking phenomenon that was catalyzed by isentropic ascent of unlocked magma. Unsorting the growth of a rim on a phase due to the last stage of evolution, for example, that of isentropic decompression, from a reactive dissolution 'new growth' signal when the crystal is undergoing net mass loss (dissolution) or possible (minor) new growth requires careful analysis based not only on phase equilibria but also an informed understanding of growth and dissolution kinetics for the appropriate phases.

#### UNLOCKING TIMESCALE ANALYSIS

Magma Apposition: Definition of Mixing, Mingling, and Hybridization

The term magma mixing typically connotes chemical mixing or at least partial chemical mixing, which is a special case of the more general process of magma

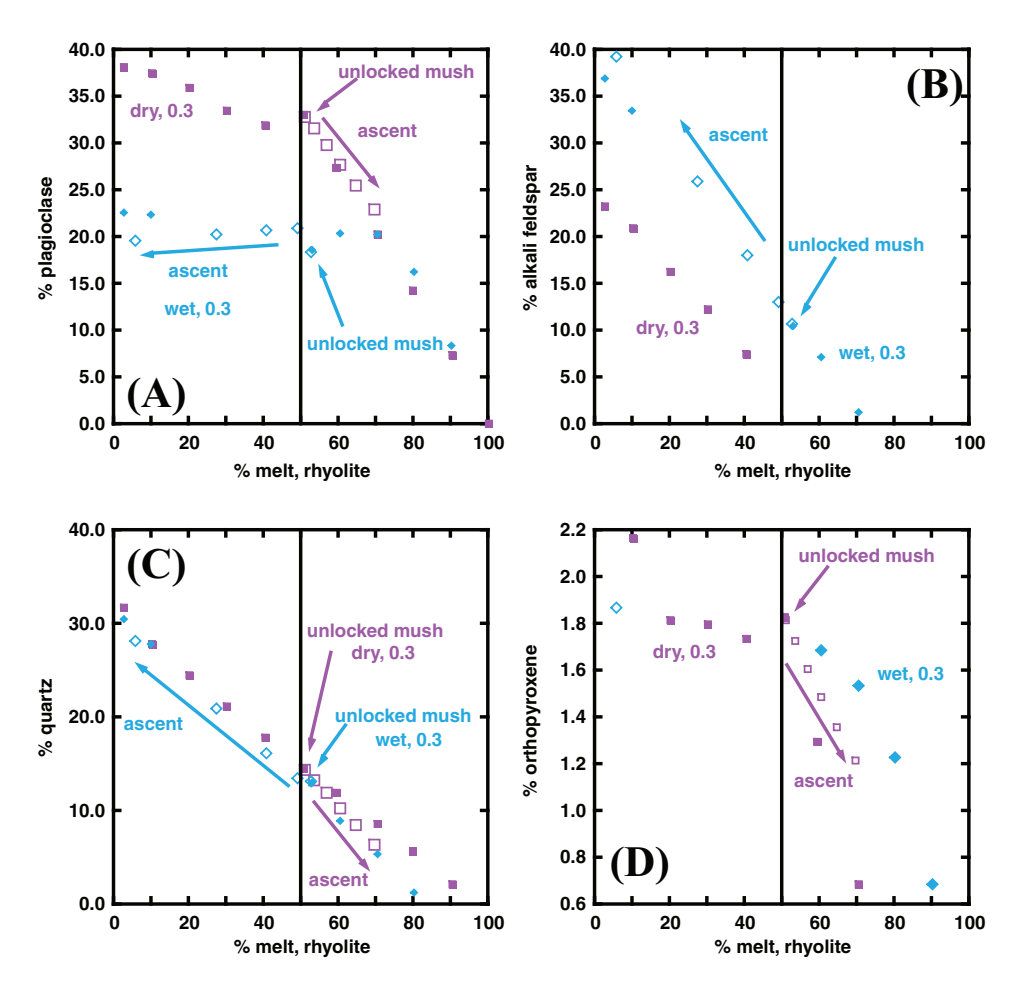


Fig. 13. Percent rhyolite melt versus percent mineral phase in mush as it unlocks (closed symbols) for same two cases described in figure 12. Open symbols represent isentropic ascent paths described in figure 12. (A) Plagioclase, (B) alkali feldspar, (C) quartz, (D) orthopyroxene. Colors same as figure 2.

apposition. The apposition of two initially distinct magmas, as used in this study, simply means two magmas are brought close enough together to enable potential interaction by the exchange of heat and/or mass and/or momentum. Of these three exchange quantities, the focus is usually placed upon heat and mass transfer, although momentum transfer can be an important mechanism for the mixing of magmas by forced (jets) or free convection.

Some basic definitions to distinguish the styles of magma apposition are useful. The term 'magma mixing' is an umbrella term encapsulating two end-member possibilities: magma mingling or magma hybridization. In *magma mingling*, there is no significant mass exchange (except for minor diffusive interfacial exchange) between **M** and **R**, although there is heat transfer. When the characteristic size of an **R** clump is small, thermal equilibration is rapidly achieved. If instead **R** is not intimately intermingled with **M**, the heat transfer timescale can be quite long. In *magma hybridization* there is complete chemical blending of the two end-member magmas. This implies that both thermal and chemical potential equilibration is achieved. The hybrid

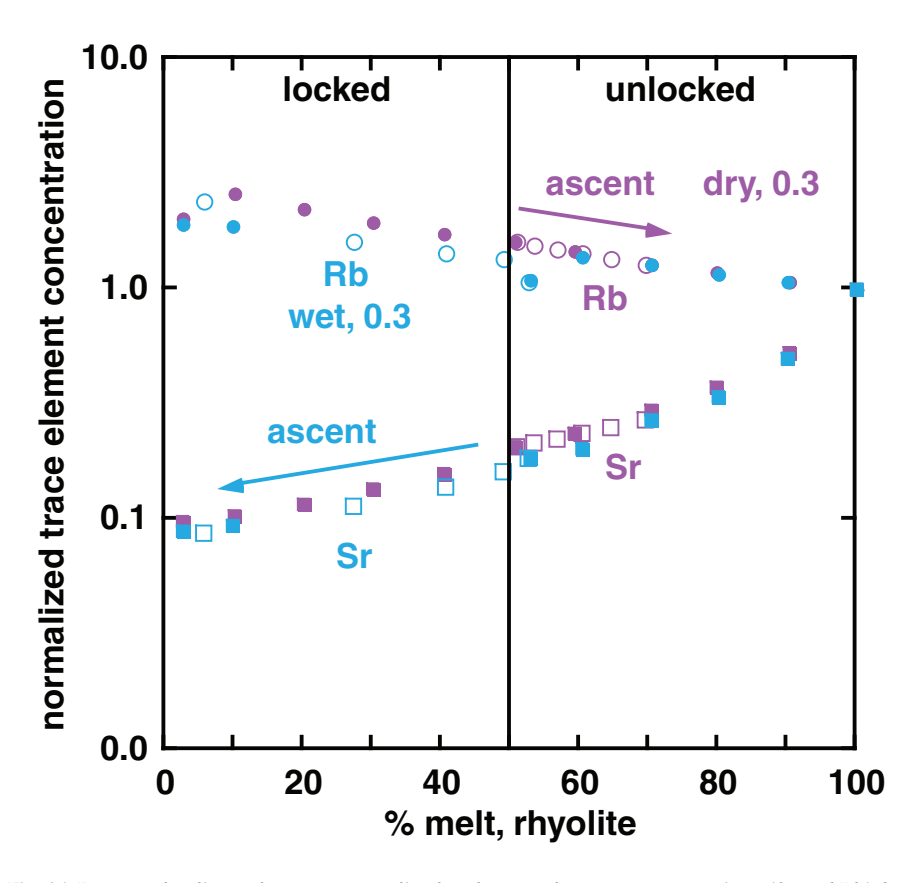


Fig. 14. Percent rhyolite melt versus normalized melt trace element concentrations (Sr and Rb) for cases described in figure 12. Closed symbols represent unlocking and open systems represent isentropic ascent. Colors same as figure 2.

magma, which may be a melt or a magma, is an equilibrium entity with no vestige of the formerly distinct end-members. Natural systems fall somewhere along the minglinghybridization spectrum. The style of magma mixing depends upon initial and boundary conditions, magma properties, driving forces, and time available for mixing. Mixing occurs via reduction of the size of compositional and rheological heterogeneities, here called R magma 'clumps', through stretching and folding by viscous flow within host **M** magma driven by release of buoyancy or by forced convection (jetting or fountaining). Once strain has reduced the size of clumps to diffusive length scales, further viscous flow accompanied by quantitatively important chemical diffusion will produce a homogenized (hybrid) magma. The approach to hybridization can be arrested at any point depending on the thermal and dynamic regimes that operate. Because the diffusion of heat is far more rapid than the diffusion of matter, it is likely that mingled magmas can be in thermal equilibrium while retaining their distinct compositional identities. Further discussion of magma mingling and magma hybridization, with an emphasis on the thermodynamics of magma hybridization may be found elsewhere (for example, Spera and others, 2016).

The Heat Exchange Problem: Clumps of Recharge Magma Distributed in Mush

Rheological unlocking of highly crystalline magma by newly apposed hotter and more mafic magma is fundamentally a heat exchange problem. For unlocking to work, there are two requirements. The first is the energy requirement, and the second is the heat transfer timescale. The energetic requirement is that sufficient heat must be available from recharge magma to unlock the silicic mush. As described above, if the initial thermodynamic states of **M** and **R** are specified, phase equilibria computations can be used to determine the quantity of heat available from **R** (and required by **M**) to achieve unlocking. From this enthalpy assessment, a mass ratio  $\Re = M_R/M_M = \rho_R V_R/\rho_M V_R$  is defined, based on isenthalpic **R**/**M** heat exchange, such that the final thermodynamic state of the **M** magma is unlocked. The efficiency of heat exchange can be factored using an efficiency factor that allows for some of the heat derived from **R** to be dissipated in the environment outside of **M**. In this work, the efficiency factor is set to unity. Therefore, the mass ratio of **R** to **M** magma needed for unlocking represents a minimum value.

The second requirement is that the thermal equilibration time, identical to the unlocking time when the energetic requirement is satisfied, must be consistent with constraints from the geologic record, specifically the volume of rejuvenated (unlocked) magma, V<sub>M</sub> (as measured by the eruptive volume), and all geokinetic and geochronological constraints from diffusion geospeedometry, zircon geochronology, and geothermometry (for example, Ti in quartz). The rate at which unlocking can be attained depends upon the transport and thermodynamic properties of M and R, notably their respective thermal conductivities, viscosities, heat capacities, and fusion enthalpies as well as the interfacial area across which heat exchange takes place. Heat exchange of a layered R below M configuration is significantly slower than in a system in which small clumps of **R** are dispersed into resident **M** magma, although the total amount of available heat may be the same. This simple geometric feature is of paramount importance and can be conveniently described as the dispersion of 'clumps' of **R** magma within **M** magma. (There is no connotation regarding the size of such clumps). By specifying the mass ratio of the discontinuous magma (typically the recharge magma) to the continuous magma (typically M magma), as well as the characteristic shape (for example, sheets, cylindrical pipes, spherical clumps, et cetera) and size of the clumps, one can evaluate the interfacial contact area.

For a given mass ratio  $\Re \equiv M_R/M_M = \rho_R V_R/\rho_M V_R$ , a characteristic length,  $L_c$ , is defined as the ratio of recharge volume  $(v_R)$  to the surface area  $(a_R)$  of a single clump of **R**. For recharge clumps of various shapes, L<sub>C</sub> v<sub>R</sub>/a<sub>R</sub> is given in Appendix B. For spherical clumps,  $L_c$  is equal to 1/3 the radius of the **R** magma clump. The volume of recharge magma  $V_R = n v_R$  where n is the number of equal-sized clumps and  $v_R$  is the volume of a single clump. With this framework, we can compare unlocking times for the following cases: (1) **R** magma is contained in one large spherical clump of radius R, and (2) **R** magma is dispersed as n smaller spherical clumps *each* of radius r. These two cases are the limits of more realistic cases for which a distribution of initial clump sizes exists and can be defined. The total volume of  $\mathbf{R}$  magma is identical in (1) and (2); the only difference is the characteristic clump size. The ratio of  $L_c$  (big clump) to  $L_c$  (small clump) is R/r. For  $V_R$  equal to 100 km<sup>3</sup>, one large 'clump' (for example, a volume of **R** of radius R=2.9 km within a contiguous volume of M), and a small clump size of 10 m, the ratio of the unlocking times from figure 15 is approximately 10,000. This idealized and admittedly simplistic example illustrates the dramatic effect of the characteristic length associated with a given volume of recharge magma. The point is that the intimacy of magma apposition is extremely important in determining the unlocking time. Below, some details are provided that relate unlocking times to eruption volumes,  $V_{M}$ .

# Unlocking Time Calculations

In the sections below, we develop two simple models to constrain unlocking timescales based on the thermal equilibration of mingled M and R. The goal is to

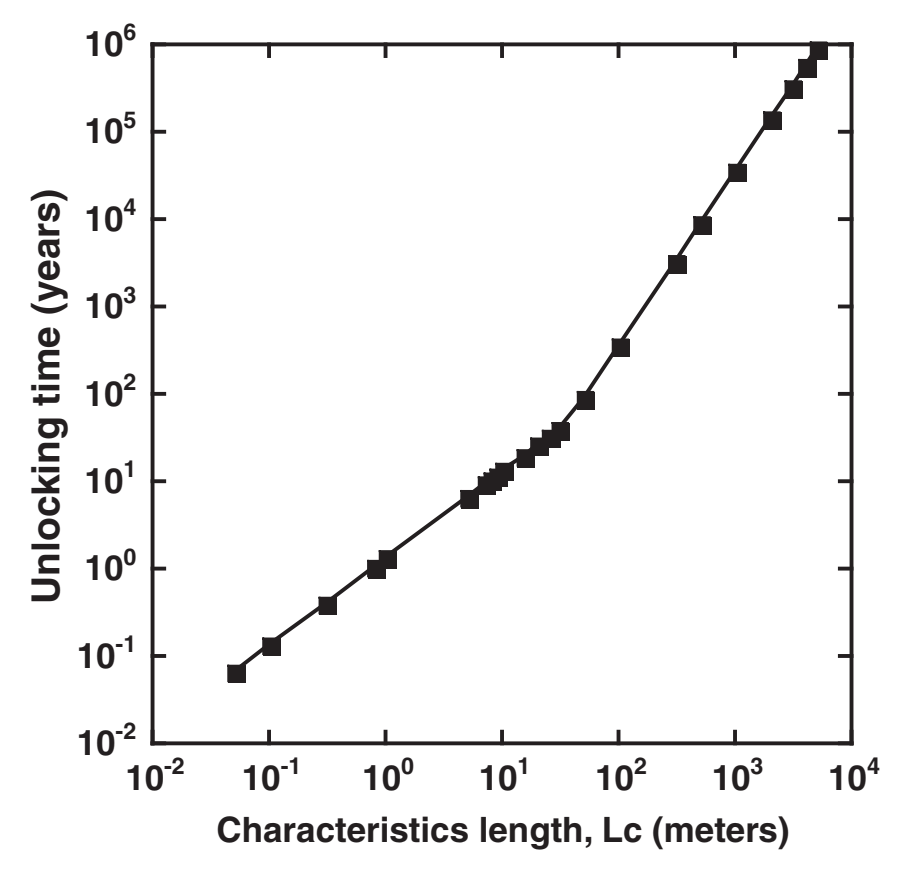


Fig. 15. Unlocking time for model 1 as a function of the characteristic length of a fixed-size clump.  $L_c$  is the ratio of clump volume to clump surface area,  $L_c = v_R/a_R$ .

present a synoptic view of the timescales for unlocking intermediate to silicic magmas in the upper crust. The models assume thermal equilibrium is attained; that is, in the final unlocked state the temperature of end-members in the mingled mixture are identical and that the heat for unlocking  $\mathbf{M}$  comes solely from  $\mathbf{R}$  with no waste heat. While these are simplifications to the behavior of natural systems, they serve the purpose of being a simply computable reference model without the need to introduce a host of other unknowns and often-unknowable considerations.

In the first model, the unlocking time is computed based on a *static* characteristic length,  $L_c$  imposed *ab initio* on the shape and size of the **R** clumps. **R** magma is the discontinuous magma distributed as clumps of characteristic linear scale  $L_c$  within **M** magma, the continuous end-member. At the unlocking time, thermal equilibrium between **R** and **M** magma is attained, and the melt fraction in **M** equals the critical threshold of 50 percent. Each of the mingled magmas retains its bulk composition and hence a phase assemblage consistent with *internal* chemical potential equilibrium consistent with the constraints from phase equilibria. The unlocking time varies with  $L_c$  linearly at small  $L_c$  and quadratically once  $L_c$  exceeds a clump size of forty meters. Figure 15 depicts this relationship and crossover length. The transition from linear to quadratic behavior depends on the assumed heat transfer coefficient between **R** and **M**, and the thermal conductivity, density, and effective heat capacity of **R**. A different

choice of parameters will change the crossover length, which can be as small as several meters but not much larger than  $\sim 50$  m. Details of the model are given in the Appendix B. The characteristic unlocking times are:

$$\tau_{unlock} = 4.6 \frac{\rho_R c_r^*}{h} L_c \text{ for } L_c \le 40 \text{ m}$$
 (1a)

$$\tau_{\rm unlock} = \frac{1}{8} \frac{\rho_R c_r^*}{k_R} \, L_c^2 \; {\rm for} \quad L_c > 40 \; m \eqno(1b)$$

The relationship between the unlocking time and  $L_c$  is given in figure 15 for the range of characteristic lengths  $L_c$  from a fraction of a meter (small clumps) to kilometers. The visual motif of clumps *per se* breaks down at large scales; a better conceptualization applicable for  $L_c \ge$  a kilometer is a contiguous volume of  $\mathbf{R}$  enclosed within a volume of  $\mathbf{M}$ .

Figure 15 shows the model dependence of unlocking time on the characteristic  ${\bf R}$  clump size. Small, order meter-sized clumps can deliver their excess heat to  ${\bf M}$  magma in a matter of a few years, whereas larger clumps, say of order 1 km, require tens of thousands of years to deliver their excess heat and unlock  ${\bf M}$ .

In order to apply the thermal unlocking analysis to natural systems, it is useful to incorporate the energetic requirement with the heat transfer requirement explicitly. The essential question is: What is the dependence of the unlocking time of a given magma volume, V<sub>M</sub>, on the intimacy of thermal contact between R and M? The question is addressed by considering the dependence of unlocking time on the size of an **R** clump (model 1) or by allowing an initially contiguous volume of **R** to undergo a reduction in size due to strain associated with convection in M during thermal equilibration. The unlocking time is estimated for V<sub>M</sub> by first determining the minimum volume of recharge magma V<sub>R</sub> needed to provide the required enthalpy for unlocking. Figure 16 presents the  $V_M - \hat{V}_R$  relationships for the four cases presented above (0.1 GPa wet and dry, 0.3 GPa wet and dry). Then, by varying the number of clumps, n, that R is broken into, the elementary clump volume and size can be determined. If a clump shape is assumed, the ratio of clump volume,  $v_R$ , to clump interfacial area,  $a_R$ ,  $L_c = v_R/a_R$  defines a characteristic linear dimension of a clump. The relationships embodied in equations (1a) and (1b) enable one to estimate the unlocking time. L<sub>c</sub> is defined for various clump shapes in Appendix B along with other model details. Results of these calculations are presented in figure 17 for the cases that bound unlocking times: wet 0.1 GPa and dry 0.3 GPa. As an example, consider the unlocking time for 100 km<sup>3</sup> of dry crystal-rich **M** magma at 0.3 GPa. If all of the energy available in  $\mathbf{R}$  is used to remobilize  $\mathbf{M}$  (that is, heat transfer efficiency factor = 1), then from figure 16,  $\sim 35 \text{ km}^3$  of **R** is required. The unlocking time depends on the mean clump size. For example, from figure 17B, if R remains as a single contiguous body, then the unlocking time is  $\sim 15$  ka. If, on the other hand, **R** breaks up into  $10^6$ equal-sized spherical clumps, the unlocking time is much shorter, of order one decade. The unlocking time is strongly dependent upon the characteristic length  $L_c$  of an **R** clump: small clumps exchange heat far more efficiently than large clumps. Examination of figure 17B suggests that the unlocking time for large volumes of dry M magmas, say 1000 km<sup>3</sup> can vary from  $\sim 10^5$  years (for n=1) to several decades (for  $n=10^6$ ). The unlocking time in this model is a minimum time since it is assumes that at the start of unlocking, as M is being heated due to apposition of R, the clumps are already in place within magma M and that all heat from R is consumed by unlocking (no waste heat).

A slightly more sophisticated model (details in Appendix B) is to allow the mean size of an **R** clump to evolve *during* the magma mingling process. In this model, **R** 

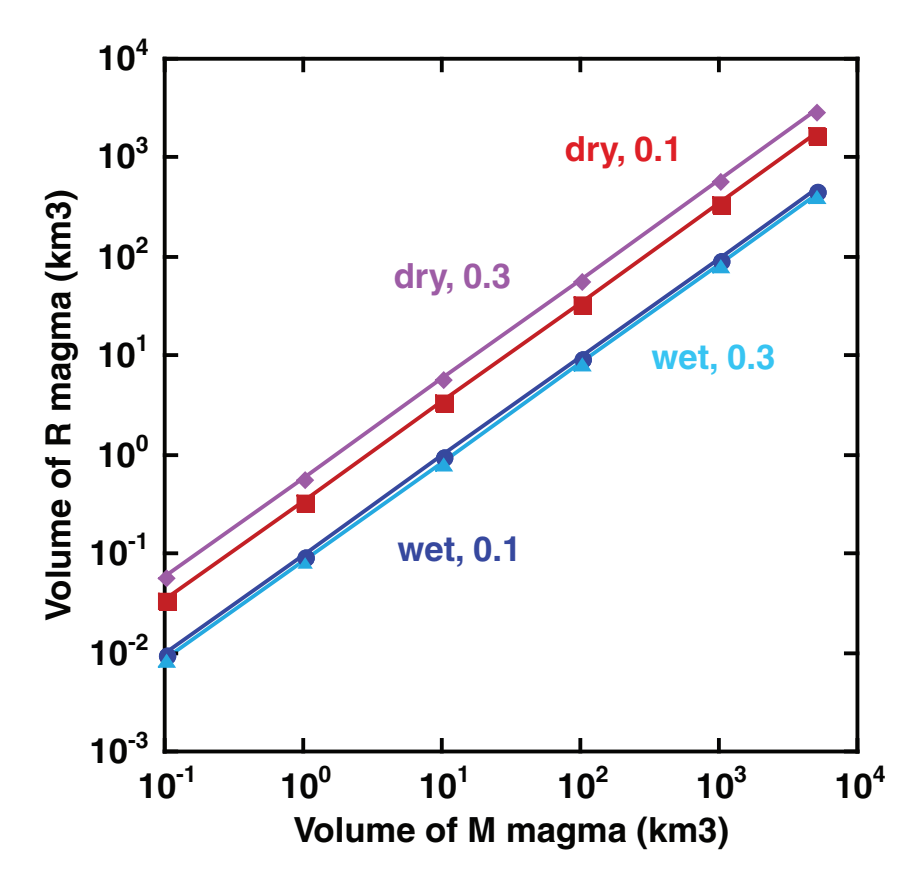


Fig. 16. Volume of **R** recharge magma  $(V_R)$  required to unlock volume of rhyolitic **M** magma  $(V_M)$ , where rhyolite starts at near-solidus condition and unlocks to 50% melt. Calculation of  $V_R$  is based on the energy that must be supplied by recharge in order to increase the melt content of **M** to the unlocking fraction of 50 wt. % melt. Rhyolite and basalt are in thermal equilibrium when rhyolite reaches the unlocked state.

magma is introduced at t=0 as a contiguous volume of characteristic linear scale  $L_c(0)$ . The reduction in clump size is taken account by considering convective motion in  $\mathbf{M}$  magma. Convection within  $\mathbf{M}$  stretches, folds and thins  $\mathbf{R}$  magma clumps from an initial linear dimension  $L_c(0)$  progressively and monotonically with time according to:

$$L_{C}(t) = L_{C}(0) \exp(-\dot{\varepsilon}t)$$
 (2)

where  $\dot{\epsilon}$  is the Lagrangian strain rate (Olson and others, 1984; Kellogg and Turcotte, 1986, 1990; Ottino, 1989; Coltice and Schmalzl, 2006) and t is the elapsed time since the start of magma mingling. In this simple model, heat exchange between **R** and **M** is concurrent with convective stretching and thinning of **R** clumps. Thermal equilibration between **M** and **R** and eventual unlocking consists of two stages: a thinning stage in which heat diffusion is negligible when  $L_c(0)$  is large in comparison to the conduction length scale followed by a later stage where, due to the progressive decrease in  $L_c$ , heat is rapidly exchanged. In cases where  $L_c(0)$  is small, the first stage is not important, and the unlocking time is given approximately by the large n limit of the previous model. The unlocking time is:

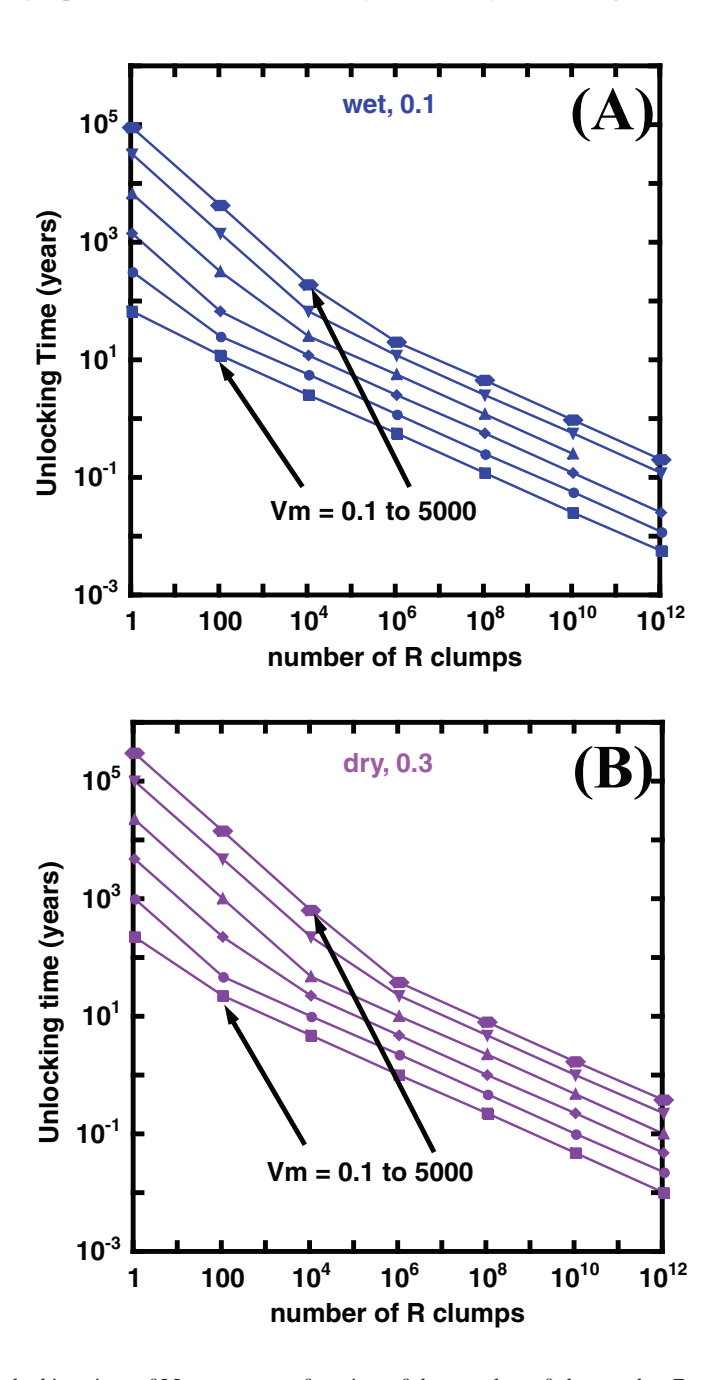


Fig. 17. Unlocking time of  ${\bf M}$  magma as a function of the number of clumps that  ${\bf R}$  magma is divided into. The clump number is given by  ${\bf n} = {\bf V}_R/{\bf v}_R$  where  ${\bf V}_R$  is the total volume of recharge apposed to  ${\bf M}$ , and  ${\bf v}_R$  is the volume of an individual clump. Systematics for various clump shapes are given in Appendix B: (A) unlocking time versus clump number for wet  ${\bf M}$  magma at 0.1 GPa, (B) unlocking time versus clump size for dry M magma at 0.3 GPa.

$$\tau_{\rm unlock} = \frac{1}{2\dot{\epsilon}} \ln \left[ 200 \frac{\rho_R C_R^* \, \dot{\epsilon} L_C^2(0)}{k_R} + 1 \right] \tag{3}$$

In order to make useful estimates of the unlocking time, the Lagrangian strain rate is parameterized using scaling results from convection theory (for example, Spera, 1992). For a volume of  ${\bf M}$  magma  $V_M$  that is undergoing convective stirring, scaling gives the strain rate as

$$\dot{\epsilon} \approx \frac{u}{V_{M}^{1/3}} \approx a_{1} \frac{k_{M}}{V_{M}^{2/3} \rho_{M} C_{M}} Ra^{2/3} \tag{4}$$

where u is the mean convective velocity and the Rayleigh number is defined

$$Ra = \frac{\rho_{\rm M}^2 C_{\rm M} \alpha_{\rm M} g V_{\rm M} \Delta T}{n_{\rm M} k_{\rm M}}$$
 (5)

Symbols appearing in all equations not defined directly in the text are given in table B2. Combining equations (3) (4) and (5) gives the unlocking time as a function of the parameters of the model:

$$\tau_{\rm unlock} = \frac{\left(\rho_{M}g\alpha\Delta T\right)^{-2/3}}{2a_{1}\kappa_{M}}\,\eta_{M}^{2/3}\,ln \bigg[\frac{200a_{1}\kappa_{M}^{1/3}\kappa_{R}(\rho_{M}g\alpha\Delta T)^{2/3}}{9\eta_{M}^{2/3}}\left(\frac{3V_{R}}{4\pi}\right)^{2/3} + 1\bigg] \tag{6}$$

Although equation 6 may appear daunting, it can be simplified by noting that many of the parameters do not vary greatly. Adopting representative values for these properties and incorporating numerical factors, equation 6 can be written in the simpler form to reveal the variables that vary the most widely in natural systems and sensibly regulate the unlocking time in this elementary model:  $\mathbf{M}$  magma viscosity,  $\eta_{\mathbf{M}}$  and recharge magma volume,  $V_{\mathbf{R}}$ :

$$\tau_{\rm unlock} = A \eta_{\rm M}^{2/3} \ln \left[ \left( \frac{V_{\rm R}}{\eta_{\rm M}} \right)^{2/3} + 1 \right] \tag{7}$$

The viscosity of **M** enters because the rate of deformation of **R** clumps depends on the convective shear strain in **M** that carries and deforms **R** clumps. As **M** undergoes partial melting, its viscosity will decrease but not in a spatially uniform way. The model is too simple to account for this, but its effect can be roughly accounted for by computing unlocking times at different **M** viscosity values (fig. 18). In order for the computed unlocking times to be relevant, note that  $V_R$  must satisfy the energetic constraint discussed in an earlier part of this paper. Figure 18 shows the variation of the unlocking time as a function of  $V_M$  for a range of **M** magma viscosities. As an example, for the case of dry **M** magma at 0.3 GPa when viscosity is  $10^{14}$  Pa s, unlocking  $1000 \text{ km}^3$  requires approximately 80 ka.

#### SYNOPSIS AND IMPLICATIONS

The goals of this section are to summarize how constraints from energetics, phase equilibria, trace element systematics, and unlocking timescale calculations inform hypotheses related to thermal rejuvenation of high-crystallinity magma bodies. This is a complex phenomenon with multiple nested spatiotemporal scales, and no single model or calculation can possibly suffice. Care must be exercised to ensure that observations used to infer unlocking times pertain specifically to rheological mobilization. To wit, there are numerous characteristic times and spatial scales relevant to the generation, segregation, ascent, storage (crystallization), unlocking and eruptive

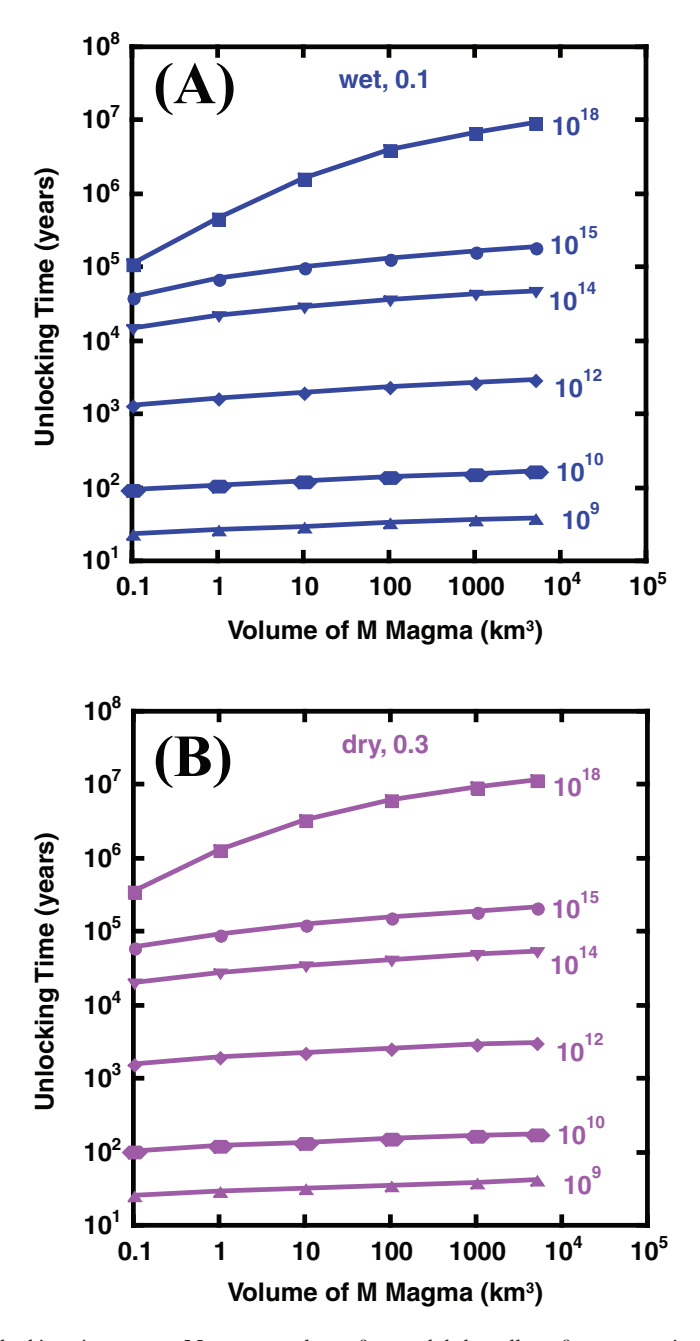


Fig. 18. Unlocking time versus  ${\bf M}$  magma volume for model that allows for progressive decrease in the characteristic length  ${\bf L}_c$  due to convective stretching and thinning of  ${\bf R}$  clumps due to convection in  ${\bf M}$  mush: (A) case for wet  ${\bf M}$  magma at 0.1 GPa, (B) case for dry  ${\bf M}$  magma at 0.3 GPa. Curves are labeled by viscosity (Pa s) of  ${\bf M}$  magma.

decompression of magma; many of these processes overlap, and it can be misleading to ascribe a single observation, such as compositionally distinct rims on phenocrysts or a set of extracted Ti-in-quartz temperatures, to unlocking unless corroborative evidence

is available. Nevertheless, decomposing the unlocking problem into an energeticphase equilibria portion and a heat transport portion is useful. Below, we summarize the constraints on unlocking developed in this study, and follow with a list of implications that provide fodder for continued study.

## Synopsis of Constraints on Unlocking

The energetic constraint is straightforward: sufficient heat must be transferred from **R** to **M** so that, given the initial thermodynamic states of **M** and **R** (for example, abundance and composition of all phases, redox conditions, mean temperatures, mean pressures), the end state of **M** must be at least  $\sim 50$  percent melt. The energetic requirement therefore defines a minimum mass of **R** for unlocking **M**. If some of the excess energy of **R** is dissipated in the environment more **R** magma is required. The tools for quantifying the energetic requirement for unlocking by magma mingling are currently available. Phase equilibria models such as Rhyolite-MELTS (Gualda and others, 2012) can handle a wide range of bulk compositions for relevant redox conditions, temperatures and pressures pertinent to the Earth's crust. Although in this study attention has been focused on magma mingling, in the limit where **R** and **M** mix to produce a single hybrid magma, the energetics of magma hybridization can be handled by the Magma Chamber Simulator model (Bohrson and others, 2014; see Spera and others, 2016 for examples). Phase equilibria models provide, along with energy constraints, mineralogical and petrographic details that can be compared with observations; discrepancies can then lead to an iterative process for refining the details of magma mixing. Phase equilibria calculations provide, in addition, a foundation upon which trace element computations can be performed and tested against observations such as zoning profiles.

Satisfying the energetic condition is not sufficient for unlocking by magma mingling. An additional condition is that heat must be transferred from **R** to **M** on a timescale consistent with geochronological, crystal stratigraphy and eruptive history observations and constraints. As noted earlier, the heat transfer problem is governed by a host of parameters related to the thermodynamic and transport properties of M and **R** as well as the geometric configuration associated with magma apposition. In particular, the total **R** to **M** interfacial area across which heat is transferred is of central importance. Heat transfer is treated here using two simple models that capture the essence of heat exchange between **R** and **M**. In both models, unlocking times vary from years to several million years, depending on  $V_M$  and the mean size of a clump (model 1) or the rate at which mean clump size is reduced through the action of stretching and folding (model 2). Most importantly, according to the view promulgated here, if large volume systems ( $V_M \sim 10-1000 \text{ km}^3$ ) are believed to be unlocked on short (year to decade) timescales, one expects to find bimodal compositions (in the case of basaltic recharge) at any given stratigraphic horizon in the volcanic deposit because only small clumps can exchange heat rapidly.

## Implications of Model Results

- 1. A fundamental requirement of mush rejuvenation is that there is sufficient enthalpy available from recharge magma (or volatiles provided by degassing of recharge magma) to partially melt the mush to an unlocked state. Thermodynamic phase equilibria models provide a way to define a mass of mingled magma (where only heat is transferred) that can unlock a crystal-rich mush. Estimating these masses is an essential first step in documenting unlocking, not only to constrain the energy exchange but also to complement geodetic and gas discharge models at potentially active volcanoes.
- 2. The energetic models presented in this study show unlocking requires a ratio of recharge to mush magma that can be less than unity. A key outcome of our

work is that unlocking of wetter rhyolitic mush is energetically favored, compared to drier counterparts; thus, (all other factors being equal), wetter mushes require smaller masses of recharge magma to achieve unlocking. This is a consequence of the fact that the bulk composition of volatile-saturated or 'wet' silicic magmas is very close to the four phase (quartz-alkali feldsparplagioclase-H<sub>9</sub>O-rich fluid) pseudoinvariant point in P-T-X thermodynamic coordinates. Hence heat from an external source such as a hot mafic intrusion goes into increasing the melt fraction within the formally locked mush that remains essentially isothermal. That is, the temperature record of unlocking is quite different for 'wet' versus 'dry' magmas. The temperature changes during unlocking of wet mush are muted, with changes from near-solidus to unlocked conditions being only a few degrees (<15 °C, Appendix A, fig. 2). In contrast, for a dry system, temperature changes during partial melting to the unlocked state may be hundreds of degrees. Therefore, geothermometry constraints may yield clear evidence of a heating event in a dry magma, whereas the up-temperature signature may be subtler or even absent in wet systems. Recognizing that the formation of mushes with higher and lower volatile contents is likely influenced by other factors, such as tectonic setting and source regions, this implication suggests that rejuvenated magmas (preserved as volcanic deposits) characterized by higher pre-eruptive fluid concentrations should be more abundant than those that are drier. A second implication is that drier unlocked, erupted mushes may be relatively restricted to tectonic settings that have higher recharge (that is, mostly basaltic) flux rates. Both of these conjectures can be tested using information on natural well-documented magmatic systems use, for example, of Ti in quartz geothermometry.

3. Phase equilibria models predict crystal growth and resorption, and changes in melt, mineral, and fluid phase masses, enthalpies and compositions during unlocking. The predictions of these and other models for a variety of initial conditions can be compared with observations in natural systems. In the four fiducial cases presented, most mineral phases decrease in abundance during unlocking. This outcome is anticipated, but phase equilibria constraints make specific quantitative predictions about phase abundance and compositional variations that can be compared to the rock record. A fundamental implication from these results is that abundant new crystallization is not predicted during unlocking, and thus, the dominant crystal texture for unlocked magmas should be resorption (or other disequilibrium textures that reflect crystal dissolution). A number of studies have clearly recognized that unlocking can lead to crystal reaction/dissolution (for example, Bachmann and others, 2002; Wark and others, 2007; Matthews and others, 2011). But, new crystallization can also be an outcome of unlocking as long as the net fraction of melt increases. Crystallization is also predicted by isentropic ascent that may follow unlocking. Our results illustrate that crystallization characteristics can be predicted, and may be different in crystals (or parts of crystals such as rims) preserved during unlocking versus ascent (and potentially other processes as well). Another source of compositional change involves phases that decrease in abundance but remain stable throughout defrosting; these may accommodate a changing thermodynamic state by reactive dissolution. That is, crystal rims may differ from cores and appear to be new growth when in fact there has been net dissolution accompanied by a change in rim composition. The phase equilibria and elemental signatures of these processes are dependent

- on a number of factors, but the point is that crystal zoning can occur in a multitude of ways, at different points in the history of a silicic magma body, and thus, the causes of zoning (or other changes in the crystal population) need to be unambiguously documented using thermodynamic phase equilibria tools.
- 4. Why is it so critical to differentiate distinct events that can lead to crystallization and/or compositional change in crystals? Because as shown in figure 1, multiple nested processes act on a magma body that reaches a near-solidus state, unlocks, and erupts, and the inevitable implication is that there are multiple associated timescales. Conflating these timescales will lead to erroneous conclusions about a range of characteristics of the magma system, not the least of which might be the timeframe over which "eruptible" magma might be generated. Distinct processes must be defined by integrating the study of whole-rock, mineral, and melt and fluid inclusion chemical data, experiments, phase equilibria modeling, energy and mass balance models, geobarometry—the gamut of tools available to the petrologist, geochemist, volcanologist—and these processes must be viewed holistically as parts of a larger group of processes that describe the development of the mush, its unlocking, ascent, and eruption.

An example of a study that thoroughly discusses the distinct timescales that can impact a rejuvenated magma body is Matthews and others (2012). The authors recognize multiple timescales associated with assembly, reactivation, magma recharge, and eruption. The reactivation timescale is defined as the time between injection of recharge magma and initiation of whole-chamber convection; for the ~1000 km<sup>3</sup> Whakamura super-eruption (New Zealand) studied by these authors, the reactivation timescale is estimated to be 10<sup>3</sup> to 10<sup>4</sup> years. Ti diffusion in quartz timescales yield the timeframe between a recharge event that records a thermal pulse in quartz and eruption, minus the time associated with crystal resorption, which is not quantified in their study. Zircons studies of Whakamura suggest magma generation and residence of over 250 ka (Brown and Fletcher, 1999 and see also discussion in Matthews and others, 2012). These authors also discuss the multistage histories preserved in quartz that are likely evidence of multiple episodes of recharge that occur in the (potential) lead up to eruption. This study is insightful in that it deconvolves the nested histories of processes that attend assembly, growth, recharge, reactivation/stirring, and eruption. Other studies provide less clarity. Published diffusion and growth/resorption studies beautifully constrain timescales, invoking sophisticated modeling techniques that lead to ever increasing insight about the associated timescales and processes. But, in some cases, the connection between the growth (or dissolution) catalyst and the process of unlocking (that is, enthalpy transfer) is ambiguous. The phase equilibria results we present above suggest first, that net crystal growth is rare during unlocking, and second, that if it does occur, then it is unlikely that the period of growth is the same as the full period of enthalpy exchange (unlocking). Similar caveats apply to crystals that have undergone or more likely undergone dissolution and reactive re-equilibration. In contrast, crystal growth may indeed occur during isentropic ascent. Timescales defined by chronometers that utilize crystal zoning characteristics (for example, diffusion) or rates of crystal growth or dissolution are unlikely to be equivalent to the timescale of unlocking (that is, enthalpy transfer). Particularly in the case where very short timescales are invoked for rejuvenation, the question that is paramount is: Are these timescales those of the unlocking or are they post-unlocking timescales? The difference between these timescales for volcano hazard monitoring and mitigation may be profound.

5. The timescale analyses presented here reflect two approaches that model enthalpy exchange only; that is, recharge magma mingles with silicic mush. In one approach, recharge magma clumps are ab initio distributed into the mush, and the timescales to thermal equilibrium and unlocking (50% melt) are evaluated; in the second, the initial condition in recharge magma is one larger clump, but through folding and stretching, clump size decreases while clump number increases. A range of unlocking timescales for both approaches is < 1 year to  $>10^6$  years. Mush viscosity also plays a role in unlocking, with stiffer magmas taking longer to unlock, other factors being equal. These timescales of unlocking are similar to those calculated using more sophisticated magma dynamical models (for example, Bachmann and Huber, 2016; Huber and others, 2010) therefore indicating that the more general approach we take provides a reliable, general guide to unlocking times. An important implication that derives from these results is that short timescales of unlocking are indeed possible, even for larger volumes of mush, but geologic evidence of the intimate interactions (many small clumps) will be evident. For example, to unlock even relatively modest magma volumes (0.1 - 1 km<sup>3</sup>) in decadal timeframes requires the relevant volume of recharge magma to be dispersed as tens to hundreds of thousands of clumps. Such effective dispersion should be recorded as abundant enclaves or mixed pumice clots in pyroclastic deposits. The counter argument is just as important; studies that suggest modest to large volumes of silicic mush can be rejuvenated in decadal to century timescales based on diffusion or other types of studies that rely on crystal growth, without abundant preservation of enclaves, are suspect.

### CONCLUSIONS

Rejuvenation of silicic mush from a near-solidus to potentially eruptible state by heat (±mass) transfer from recharge magma is a paradigm that effectively addresses a range of observations, experimental results, and model predictions. While not all silicic magmas likely undergo rejuvenation subsequent to cooling and crystallization to mush, abundant thermochemical evidence supports the occurrence of unlocking in silicic magma systems. This is a natural consequence of the ultimate enthalpy transport process giving rise to crustal magma bodies: heat derived from the upward advection of mantle heat by ascending melt generated by partial fusion of ultramafic and eclogitic source rocks. The chronology of processes and timescales that can affect a crustal silicic magma body as it forms, crystallizes (±crustal assimilation, magma mixing, volatile exsolution), cools to a near-solidus state, unlocks, ascends, and erupts presented here highlights the multiplicity of nested processes and timescales that can be recorded by melt, crystals, and melt and fluid inclusions in plutonic and volcanic rocks. Thermodynamic and heat transport calculations describing the physiochemical changes that a silicic magma body undergoes as it unlocks and potentially ascends and erupts are an essential step in correctly interpreting timescales derived from crystal characteristics.

### **ACKNOWLEDGMENTS**

The National Science Foundation provided support to both FJS and WAB for this work. We thank Mark Ghiorso for the invitation to contribute to this volume. We gratefully acknowledge the comments, insights, and corrections provided by Catherine Annen and Robert Wiebe.

APPENDIX A
TABLE A1\_1
Dry 0.1 GPa

				Dr	Jry 0.1 GPa						
Rhyolite	100 % melt	90 % melt	80 % melt	70 % melt	60 % melt	50 % melt	40 % melt	30 % melt	20 % melt	10 % melt	3 % melt (near solidus)
Rhvolite temperature (°C)	987.11	949.11	935.11	925.11	911.11	901.11	881.11	855.11	809.11	745.11	737.11
Rhyolite system enthalpy (J)	-1331393.67	-1338415.63	-1342080.22	-1344851.88	-1348469.75	-1351597.27	-1356077.74	-1360964.99	-1368	-1377	-1379737.01
Rhyolite % crystals	0	10	20	29	41	49	09	70			
Rhyolite % liquid	100	06	80	71	59	51	40	30	20	8	3
Rhyolite % fluid	0	0	0	0	0	0	0	0			0
enthalpy difference per 100											
grams from near solidus (J)	48343.34	41321.38	37656.79	34885.13	31267.26	28139.74	23659.27	18772.02	114	17	
plagioclase		9.72	16.28	21.77	20.1	23.46	28.34	32.13			7
orthopyroxene			0.53	1.03	1.65	1.36	1.49	1.57	1.62	1.91	
quartz			3.52	6.53	10.25	13.39	17.17	20.48			
alkali feldspar					8.7	10.54	12.34	14.35			(4
spinel						69.0	1.05	1.33			
ilmenite										0.3	0.32
apatite										0.17	
H <sub>2</sub> O fluid phase											
SUM crystals		9.72	20.33	33	0.7	4.6	50.3	98.69	79.9	91.85	97.22
Basalt		100 % melt	90 % melt	80 % melt	70 % melt 60	60 % melt 50	50 % melt 40	40 % melt 30	30 % melt 20	20 % melt 10	10 % melt
Rhyolite temperature (See above)		987.11	949.11	935.11	925.11	911.11	901.11	881.11	855.11	809.11	745.11
Basalt temperature (°C)	1148.44		950.44	934.44	924.44	910.44	900.44	880.44	854.44	808.44	744.44
Basalt enthalpy	-1172320.85	-12193	-1226953.86	-1230032.29	7		$\overline{}$				-1263355.48
Basalt % crystals	0		61.19	65.83	71.8	80.36	83.78	86.83	89.35	91.48	96.2
Basalt % liquid	100	47.97	37.94	34.17	28.2	19.64	16.22	13.17	10.65	8.52	3.8
Basalt % fluid phase		0.82	1.18	1.32	1.4	1.51	1.56	1.64	1.7	1.72	1.84
Basalt enthalpy available from		47007.01	54633.01	57711.44	61379.95	86529.98	69172.89	72425.81	76196.56	82570.01	91034.63
liquidus (J per 100 grams)											
Basalt mass ratio required to reach		1.03	0.76	0.65	0.57	0.47	0.41	0.33	0.25	0.14	0.02
thermal equilibrium											
olivine		7.58	8.95	9.38	6.5	1.73					
spinel		10.82	10.94	10.92	12.04	13.8	14.26	14.08	13.84	13.14	10.18
clinopyroxene		23.48	24.15	24.45	24.36	24.5	24.88	24.59	24.33	24.66	24.05
H <sub>2</sub> O fluid phase		0.82	1.18	1.32	1.4	1.51	1.56	1.64	1.7	1.72	1.84
plagioclase		9.18	16.7	19.55	23.65	29.46	31.65	33.98	35.84	36.83	38.74
apatite		0.15	0.45	0.54	0.67	98.0	0.93	1	1.05	1.09	1.2
biotite					3.51	8.89	10.88	11.92	12.95	14.4	15.84
alkali feldspar											2.1
ilmenite											2.59
SUM crystals		51.21	61.19	64.84	70.73	79.24	82.6	85.57	88.01	90.12	94.7

Table A1\_2
Wet 0.1GPa

					Wet 0.1GPa	π					
Rhyolite	100 % melt	90 % melt	80 % melt	70 % melt	60 % melt	50 % melt	40 % melt	30 % melt	20 % melt	10 % melt 3	3 % melt (near solidus)
Rhyolite temperature (°C)	855.08	803.08	763.08		751.08			749.08	747.08	743.08	737.08
Rhyolite system enthalpy (J)	-1343625.66	-1353188.34	-1360370.96		-1364826.24			-1369529.38	-1372187.60	-1373970.96	-1375152.82
Rhyolite % crystals	0	10	19		37			29	83	91	94
Rhyolite % liquid	100		80		61			31	14	5	3
Rhyolite % fluid	0	0	0.68		1.46			2.68	3.33	3.67	3.78
enthalpy difference per 100											
grams from near solidus (J)	31527.16	21964.48	14781.86		10326.58			5623.44	2965.22	1181.86	
plagioclase		8.61	16.9		19.64			19.01	19.29	19.66	19.94
orthopyroxene			0.0		1.19			1.61	1.79	1.87	1.9
quartz					7.2			18.8	25.07	28.35	29.38
alkali feldspar					7.89			25.88	34.93	39.44	40.68
spinel		1.18	1.27		1.41			1.3	1.31	1.31	1.31
ilmenite								0.2	0.26	0.3	0.31
biotite											0.01
leucite		0.28	89.0		1.46			2.68	3.33	3.67	3.78
fluid		9.79	19.07		37.33			8.99	82.65	90.93	93.53
SUM crystals	855.08	803.08	763.08		751.08			749.08	747.08	743.08	737.08
total sum	-1343625.66	-1353188.34	-1360370.96		-1364826.24			-1369529.38	-1372187.60	-1373970.96	-1375152.82
Basalt		100	100 % melt 90	90 % melt 80	80 % melt 70 % melt	melt 60 % melt	nelt 50 % melt	lt 40 % melt	30 % melt	20 % melt	10 % melt
Rhyolite temperature (See above)	(e)		855.08	803.08	763.08	7:	751.08		749.08	747.08	743.08
Basalt temperature (°C)		1148.44	854.44	804.08	764.44	7.	752.44		750.44	748.44	744.44
Basalt enthalpy (J)	-11	72320.85	-1248517.41 -12		-1260866.22	-1262366.93	56.93		-1262614.86		-1263355.48
Basalt % crystals		0	88.01	90.23	93.83		94.39		94.46	94.54	94.7
Basalt % liquid		100	10.65	8.41	4.69		4.11		4.02	3.95	3.8
Basalt % fluid phase		0	1.7	1.72	1.82		1.83		1.83	1.84	1.84
Basalt enthalpy available from liquidus (J	liquidus (J										
per 100 grams)			76196.56	83111.79	88545.37	7006	90046.08		90294.01	90541.4	91034.63
Basalt mass ratio required to reach	ach										
thermal equilibrium			0.41	0.26	0.17		0.11		90.0	0.03	0.01
olivine											
spinel			13.84	13.08	10.76		10.41		10.35	10.3	10.18
clinopyroxene			24.33	24.7	24		24.03		24.04	24.04	24.05
plagioclase			35.84	36.85	38.59		38.68		38.69	38.71	38.74
apatite			1.05	1.09	1.18		1.19		1.19	1.19	1.2
biotite			12.95	14.51	15.43		15.66		15.7	15.75	15.84
alkali feldspar					1.63		1.96		2	2.03	2.1
ilmenite					2.24		2.46		2.49	2.52	2.59
$H_2O$ fluid phase			1.7	1.72	1.82		1.83		1.83	1.84	1.84
SUM crystals			88.01	90.23	93.83		94.39		94.46	94.54	94.7

Khyolite	100 % melt	90 % melt	80 % melt	70 % melt	60 % melt	50 % melt	40 % melt	30 % melt		20 % melt 1	10 % melt 3	3 % melt (near solidus)
Rhyolite temperature (°C)	1011.52	991.52	977.52	967.52	953.52	939.52	2 921.52		893.52	845.52	751.52	691.52
Rhyolite system enthalpy (J)	-1320234.88	-1324777.71	-1328448.59	-1331460.84	-1335	-1338	-1342	-1348	Ċ		-1369237.56	-1378735.20
Rhyolite % crystals	0	86	20.1	7 00							90.1	07.4
Physlite % Liquid	0 00	2.00	70.07	207					30.1	10.01	100	7
Miyotite /0 fiquid	9.66	2.06	6.61	C.O.		,		,	100	9.61	0.0	7 0
Khyolite % fluid	0.0	0.0	0.0	0.0			_		0.0	0.0	0.0	0.7
enthalpy difference per 100	58500.32	53957.49	50286.61	47274.36	43590.26	5 40316.51	1 35914.76	5 30462.73	2.73	22667.14	9497.64	
grams from near solidus (J)												
plagioclase	0.1	7.5	14.36	20.38	2,		(°)	33	33.55	36	37.51	38.28
orthopyroxene				0.69		3 1.83			1.8	1.82	2.17	
quartz		2.27	5.78	8.66	11.95	5 14.57	_		21.21	24.59	27.86	31.77
alkali feldspar							7.51		12.32	16.31	21.03	23.3
spinel							0.64		1.05	1.42	1.14	2
ilmenite											0.36	0.27
biotite												1 27
lancita												12:1
Fucile 6:4												0.00
ıınıa											0	0.21
SUM xtals	0.1	9.77	20.14	29.73					69.93	80.14	90.07	97.42
total sum	100.0	100.0	100.0	100.0		100.0	0 100.0		100.0	100.0	100.0	100.1
Basalt		10	100 % melt 90	% melt	80 % melt 70 %	70 % melt 60 %	60 % melt 50 % melt		40 % melt	30 % melt	20 % melt	10 % melt
Rhyolite temperature (See above	ve)		1011.52	991.52	977.52	967.52		939.52	921.52	893.52	845.52	
Basalt temperature (°C)		1160.35	1012.35	992.35	978.35	968.35	954.35	938.35	922.35	894.35	846.35	752.35
Basalt enthalpy (J)	-11	63780.86	-1206877.57 -12	-1210917.99 -121	-1213568.25 -121	-1215387.14 -1217	-1217846.55 -12220	-1222057.78 -1227	227732.23	-1233971.57	-1242944.61	-1256417.69
Basalt % crystals		0	42.4	45.26	47.02	48.15	49.57	55.04	63.13	86.69	78.66	89.85
Basalt % liquid		100	58	55.06	53.29	52.17	50.75	45.31	37.27	30.43	21.5	
Basalt % fluid phase		0	0	0	0	0	0	0	0	0	0.26	
Basalt enthalpy available from liquidus	lianidus		43096.71	47137.13	49787.39 5	51606.28 5	54065.69 58	58276.92 63	63951.37	70190.71	79163.75	9263
(100 grams) (J)												
Basalt mass ratio required to reach	ach		1.36	1.14	1.01	0.92	0.81	69.0	0.56	0.43	0.29	0.10
thermal equilibrium												
olivine			4.71	4.67	4.65	4.64	4.63	4.58	1.38			
spinel			10.88	11.42	11.72	11.91	12.14	11.67	12.45	12.37	12.33	9.58
clinopyroxene			26.73	29.09	30.5	31.41	32.55	30.58	28.56	26.64	25.8	
plagioclase								5.46	12.35	17.65	24.94	31.92
anatite			0.08	0.08	0.15	0.10	0.05	0.35	0.40	0.50	0.71	
apariic			00.0	00.0	0.10	0.10	9.0	55.0	0.5	10.84	14 11	16.96
alkali feldsnar									:	10.01	11:1:1	00.01
ilmenite												
orthopyroxene										1.89	0.77	3.14
H <sub>2</sub> O fluid phase											0.26	
CITA		c										

1ABLE A1\_4

17\_4 0 2 CB\_

			Wet 0.3 GPa	GPa					
Rhyolite		100 % melt	90 % melt	80 % melt	70 % melt	60 % melt	50 % melt	10 % melt	3 % melt
Rhyolite temperature (°C)		858.4	816.4	768.4	740.4	718.4	706.4	702.4	692.4
Rhyolite system enthalpy (J)		-1334865.71	-1343163.10	-1351671.19	-1357089.96	-1361600.81	-1365265.77	-1373140.21	-1375761.96
Rhyolite % crystals		0.0	6.6	20.0	29.8	39.8	47.3	87.3	94.0
Rhyolite % liquid		100.0	90.1	80.1	70.2	60.3	52.8	6.7	2.5
Rhyolite % fluid		0.0	0.0	0.0	0.0	0.0	0.0	3.	3.6
enthelmy difference ner 100 grams from near solidus (I)		30807	33 805 65	77 00017	18672 00	14161 15	10406 19	27 1090	2
characters for 100 grams non-near sonder (3)		700001	08.90	16.25	20.77001	200	10.70	27.1202	13 66
piagrociase			24.8	10.33	20.32	20.3	18./2	22.43	77.07
orthopyroxene			69.0	1.23	1.54	1.69			
quartz				1.29	5.44	9.01	13.07	27.93	30.59
alkali feldspar					1.29	7.27	10.57	33.57	36.96
spinel			0.78	1.08	1	1	1.78	1.95	1.94
ilmenite					0.21	0.29	0.19	0.24	0.26
apatite									
biotite							0.92	1.14	1.22
leucite							2.03		0.32
H <sub>2</sub> O fluid phase								3.14	3.62
SUM xtals			68.6	19.95	29.8	39.76	47.28	87.26	93.96
Basalt		100 % melt	90 % melt	80 % melt	70 % melt	60 % melt	50 % melt	10 % melt	3 % melt
Rhyolite temperature (See above)		858.4	816.4	768.4	740.4	718.4	706.4		
Basalt temperature (°C)	1160.35	858.35	816.35	768.35	740.35	718.35	706.35		
Basalt enthalpy (J)	-1163780.86	-1240683.74	-1247888.58	-1254478.65	-1257786.35	-1260057.26	-1261107.18		
Basalt % crystals	0	75.8	83.76	88.58	90.77	92.61	93.84		
Basalt % liquid	100	24.61	15.94	10.64	8.22	6.17	4.81		
Basalt % fluid phase	0	0.02	0.7	1.12	1.3	1.43	1.51		
Basalt enthalpy available from liquidus (J per 100		76902.88	84107.72	90697.79	94005.49	96276.4	97326.32		
grams)									
Basalt mass ratio required to reach thermal equilibrium		0.53	0.39	0.27	0.20	0.15	0.11		
olivine									
spinel		12.39	11.89	10.35	8.89	7.27	80.9		
clinopyroxene		25.8	26.11	26.93	27.54	28.09	28.44		
plagioclase		22.59	28.83	31.53	32.1	32.27	32.28		
apatite		0.64	0.84	0.95	1	1.06	1.1		
biotite		13.45	15.26	16.52	17.35	18.27	19		
alkali feldspar									
ilmenite									
orthopyroxene		0.93	0.83	2.3	3.89	5.65	6.94		
H <sub>2</sub> O fluid phase		0.02	0.7	1.12	1.3	1.43	1.51		
SUM crystals		75.8	83.76	88.58	90.77	92.61	93.84		

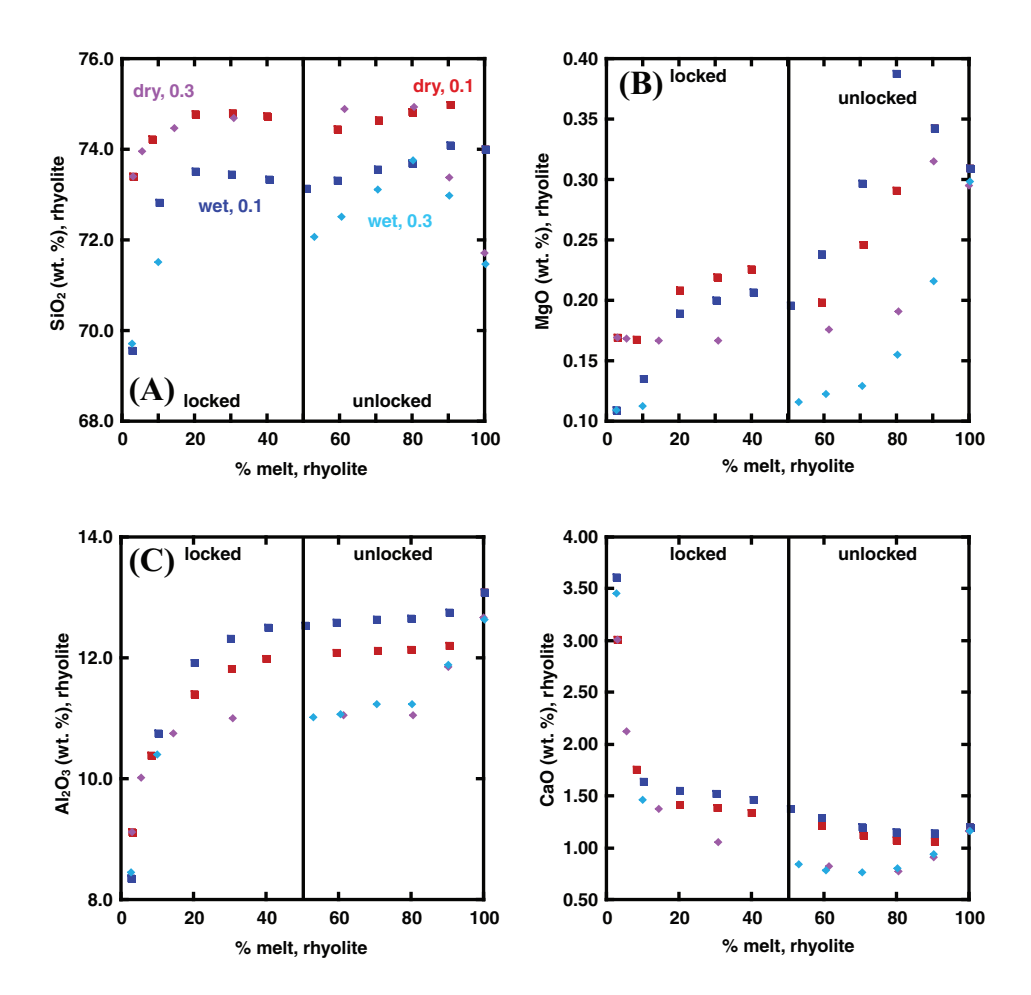


Fig. A1. (A-I) Percent rhyolite melt, from near solidus conditions to 100% melt versus select major element trends of rhyolite melt. Four cases shown. Colors same as in figure 2 (in text).

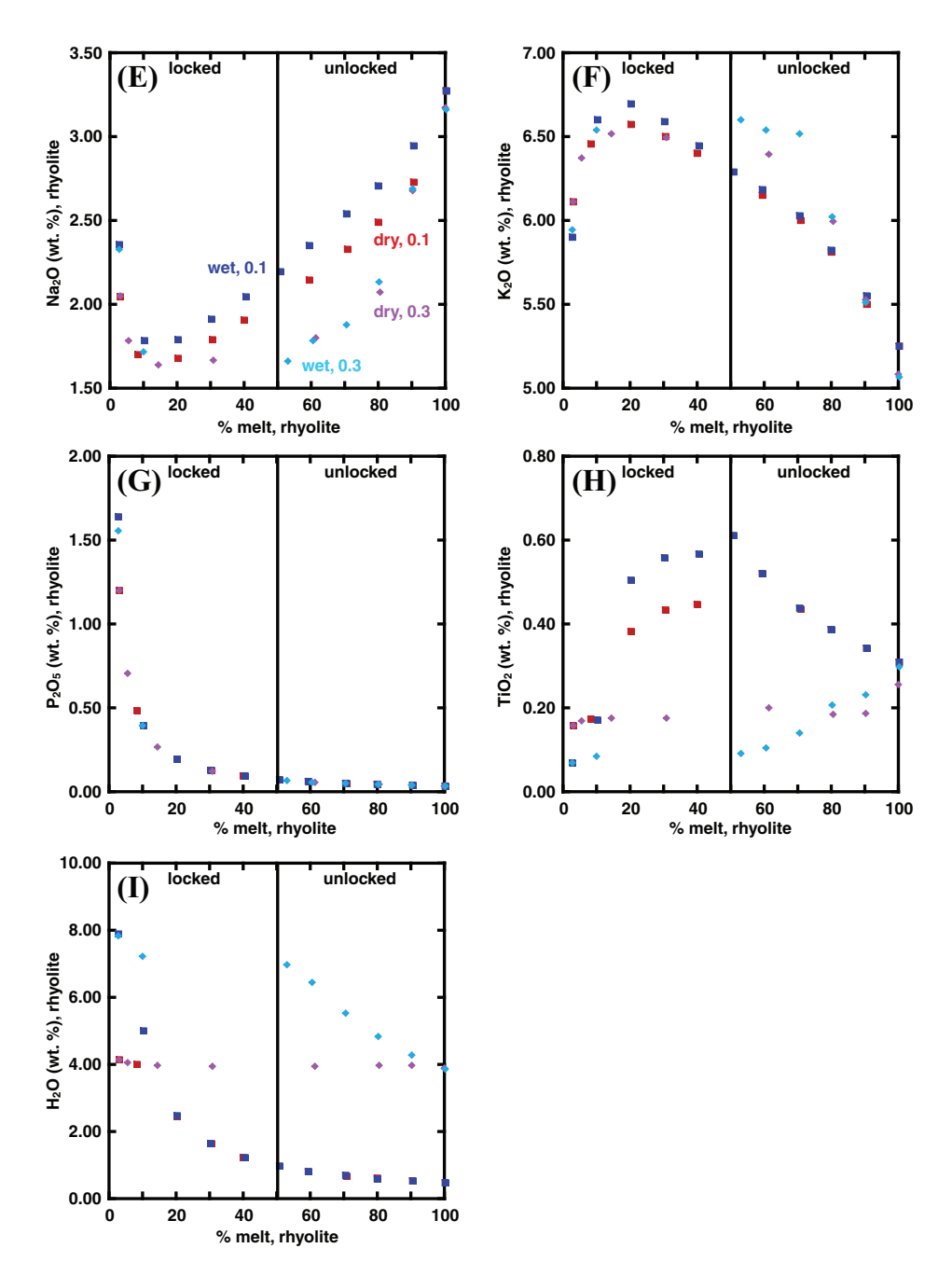


Fig. A1. (continued).

#### APPENDIX B

#### THERMAL UNLOCKING TIME MODELS

Two models are presented for the calculation of unlocking times by transport of heat from  ${\bf R}$  to  ${\bf M}$  magma. In each model, the energetic constraint for the needed available heat is met *ab initio*. When the energetic criterion is met, the thermal equilibration time is equivalent to the unlocking time. The first model is a static clump size model: at t=0 clumps of  ${\bf R}$  magma of fixed characteristic linear dimension  $L_c$  are uniformly distributed in  ${\bf M}$  and the time required for unlocking  ${\bf M}$  is determined from the heat transfer calculation. In the second model, a single large  ${\bf R}$  clump of characteristic linear dimension  $L_c(0)$  is introduced into  ${\bf M}$  magma at t=0 and heat is exchanged as the clump dynamically decreases in size by stretching and folding due to convective strain in host  ${\bf M}$  mush. The convective state of  ${\bf M}$  is given by the magnitude of the Rayleigh number given below. In both models, the energetics to accomplish unlocking is governed by the initial thermodynamic state of  ${\bf M}$  and  ${\bf R}$  and the mass ratio  ${\bf M} \equiv {\bf M}_R/{\bf M}_M = {\bf \rho}_R {\bf V}_R/{\bf \rho}_M {\bf V}_R$ . The final state of the system consists of mingled  ${\bf R}$  and  ${\bf M}$  magmas that retain their compositional distinctness but are thermally equilibrated. The timescale to achieve thermal equilibration is equivalent to the unlocking time. These models are considered in turn.

Model 1: Static Clump Size.—Consider an elementary volume  $(v_R)$  or a 'clump' of recharge magma  $(\mathbf{R})$  of arbitrary shape, mass  $m_R$ , volume  $v_r$ , surface area  $a_r$ , density  $\rho_R$ , and specific effective isobaric heat capacity  $C_R^*$ , initially at a uniform temperature  $T_R^\circ$ . The total volume of recharge magma is  $V_R = nv_R$  where n is the number of discrete clumps that come into thermal equilibrium with crystal-dominated mush of mass  $M_M$ , volume  $V_M$  and density  $\rho_M$ . Properties of  $\mathbf{M}$  are subscripted with M. The effective heat capacity includes the contribution from latent heat that is spread across the solidus to liquidus interval.

A characteristic linear dimension of a clump of  ${\bf R}$  is defined scale  $L_c = v_R/a_R$ . The total volume of recharge magma is  $V_R$ ; therefore the number of blobs is  $n = V_R/v_R$ , where  $v_R$  is the volume of an elementary volume of  ${\bf R}$  magma. The solution for the unlocking time in this model is given in two parts. For interactions where the ratio of the characteristic length,  $L_c$  is less than a critical value  $L_c^*$  (to be determined), the heat exchange rate can be estimated using a 'lumped parameter' solution (Kaviany, 2002) provided the Biot number is less than or equal to  $\sim$ 0.5. The dimensionless Biot number defined Bi  $= \frac{L_c/k_R}{1/h}$  is the ratio of conductive resistance within the clump to convective resistance at the surface of the clump. Setting the critical Biot number to 0.5, the thermal conductivity to  $k_R = 1$  W/m s K (Lesher and Spera, 2015) and  $h = 1.25 \times 10^{-2}$  Wm $^{-2}$ K $^{-1}$  (Bird and others, 1960), the crossover characteristic length  $L_c * = 40$  m.

# Thermal model: small Biot number limit ( $L_c < 40 \text{ m}$ ).

At time t=0, the body is placed into a medium at uniform temperature  $T_M^o$  and heat flows from the hot recharge magma (**R**) to the cooler, rheologically locked resident magma (**M**) with a heat transfer coefficient h. We apply a lumped system analysis so that the temperature remains uniform (no spatial gradients) in  $v_R$  at all times and changes with time only, T(t). An energy balance under these assumptions leads to the solution

$$\frac{T_{R}(t) - T_{M}^{o}}{T_{0}^{o} - T_{M}^{o}} = \exp(-Bi \text{ Fo})$$
 (B1)

with the Biot and Fourier numbers defined

$$Bi = \frac{hL_c}{k} \text{ and Fo} = \frac{k_R t}{\rho_R C_R^* \, L_c^2} \tag{B2} \label{eq:Bi}$$

The effective heat capacity of the clump accounts for both sensible cooling and latent effects as  $\mathbf{R}$  cools and crystallizes and is defined by

$$C_R^* = C_R + \Delta H / \Delta T_{s \to l}$$
 (B3)

where the first quantity on the right-hand side is the specific isobaric heat capacity of the melt of  ${\bf R}$  and the second term, the ratio of the heat of fusion divided by the solidus to liquidus temperature interval, accounts for crystallization of  ${\bf R}$ .

Once temperature of  ${\bf R}$  is available from Eq (B1), the rate of heat flow (W = J/s) between  ${\bf R}$  and  ${\bf M}$  can be determined according to

$$\dot{Q} = hA_s[T_R(t) - T_M^o] \tag{B4}$$

The total heat transferred between  $\mathbf{R}$  and  $\mathbf{M}$  over the time interval t=0 to t is the change in energy content of the  $\mathbf{R}$  blob:

$$Q = \rho_R V_R C_R^* \left[ T_R^o - T_R(t) \right] \tag{B5}$$

The heat transfer total exchange between blob of R and surrounding M magma is

$$Q_{\text{total}} = \rho_R V_R C_R^* \left[ T_R^o - T_{eq} \right]$$
 (B6)

where  $T_{\rm eq}$  is the final temperature of the composite system at thermal equilibrium. The thermal equilibration time which is identical to the unlocking time  $\tau_{\rm unlock}$  is defined as the time required for the difference in temperature between  ${\bf R}$  and  ${\bf M}$  to be 1 per cent of the initial difference  $T_R^o - T_M^o$ . The time scale is

$$\tau_{\rm unlock} \approx 4.6 \frac{\rho_R C_R^*}{h} L_c$$
(B7)

which is identical to equation (1a) in the text. The coefficient in eq (B7) arises because we assume thermal equilibration when the temperature of  $\mathbf{M}$  and  $\mathbf{R}$  are equal to within 1% in the model.

Thermal model: large Bi number limit ( $L_c > 40 \text{ m}$ )

In the limit  $Bi\gg 1$ , the interfacial thermal resistance is small relative to the thermal resistance within the R clump. In the limiting case where the interfacial thermal resistance is very large case, the temperature of the interface,  $T_s$ , is constant, essentially equal to the ambient temperature of M at large distance from the interface,  $T_M^o$ . This represents an extreme case that considers the R clump boundary is bathed by well-mixed M magma and remains constant. Although the boundary stays at a fixed temperature heat is indeed transferred from R to M. This heat transfer problem can be solved for various R clump shapes. Detailed solutions however indicate that the effect of clump shape is not large small, changing equilibration times by not more than a factor of two or three for equant, cylindrical or spherical clumps (Schneider, 1955; Carslaw and Jaeger, 1959). Because our interests lie in orders-of-magnitude given the fundamental uncertainties and simplifications, the solution for a large flat plate of uniform thickness  $L_c$  is used to evaluate this particular limiting case. The energy equation is written

$$\frac{\partial T}{\partial t} = \kappa_R \nabla^2 T \tag{B8}$$

with initial and boundary conditions  $T=T_R^o$  at  $t=0 \ \forall X\ 0\geq X\geq L_C$ ,  $T=T_R^o$  at x=0 for t>0 and  $T=T_M^o$  at  $x=L_c$  for t>0. The solution to the energy equation is

$$\frac{T - T_M^o}{T_R^o - T_M^o} = \frac{4}{\pi} \sum_{n=1}^{\infty} \frac{1}{n} \sin\left(\frac{n\pi}{L_c}x\right) \exp(-n\pi/2)^2 \text{ Fo} \quad n = 1, 3, 5, \tag{B9}$$

The heat flow from R to M is

$$\dot{Q} = 4 \left(\frac{k a_r}{L_c}\right) (T_M^o - T_R^o) \sum_{n=1}^{\infty} cos \left(\frac{n \pi x}{L_c}\right) exp \left(-\frac{n \pi}{2}\right)^2 \text{ Fo} \quad n = 1, 3, 5 \dots \tag{B10}$$

The most general case involves significant internal and interfacial thermal resistances. In this case, eq (B8) remains the same with initial and boundary conditions  $T = T_R^o$  at  $t = 0 \ \forall x \ 0 \le x \le L_C$ ,  $\frac{\partial T}{\partial x} = 0$  at centerline of R and  $\frac{\partial T}{\partial x} = \frac{h}{k} \ (T - T_M^o)$ . The solution to the energy equation is

$$\frac{T-T_{M}^{\ o}}{T_{R}^{\ o}-T_{M}^{\ o}}=2\sum_{n=1}^{\infty}\frac{\sin\,\delta_{n}cos(\delta_{n}x/L_{c})}{\delta_{n}+\sin\,\delta_{n}\cos\delta_{n}}e^{-\delta_{n}^{2}F_{0}}\ \text{and}\ \delta_{n}\ \text{is defined by}\ \delta_{n}\ \tan\,\delta_{n}\!=\!\frac{hL_{c}}{k} \tag{B11}$$

The complex nature of (B12) is best dealt with using graphical solutions as presented in the literature such as Ingersoll and others (1948) for arbitrary heat transfer coefficient h. For purposes here we used the large Bi solution which gives the unlocking time valid for  $L_c > 40 \text{ m}$  as

$$\tau_{\rm unlock} \approx \frac{1}{8} \frac{\rho_R C_R^*}{k_{\scriptscriptstyle R}} L_c^2 \ {\rm for} \ L_{\scriptscriptstyle C} > 40 m \eqno(B12)$$

which is identical to equation (1b) in the text.

The relationship between  $L_c$  and geometry of particular clump sizes and shapes is given in table B1. The number of clumps is found by dividing the total volume of recharge magma  $V_R$  by the volume of a single clump,  $v_R$ . As an example, contrast the number of clumps implied by assuming that the clump shape is taken as either a sphere of radius r or as a rectangular parallelepiped with a depth equal to length  $(z=\ell)$  and the length to width (w) aspect ratio  $\alpha=\ell/w$  (see table B1 below). For the spherical clump of radius r,  $L_c=r/3$  while a clump in the form of a rectangular volume  $L_c=\alpha w/2(\alpha+2)$ . In either case, the number of clumps is given by  $n=V_R/v_R$ . If r=10 m and w=10 m with  $\alpha=50$  (that is, dike is one hundred times longer and deeper than wide), then for, say,  $V_R=1$  km³ the number of spherical clumps is  $n\approx200,000$  whereas if R is assumes the form of dikes,  $n\approx100$ . The corresponding values for  $L_c$  are:  $L_c=3.3$  m (multiple spherical clumps) and  $L_c=4.8$  m (multiple dikes).

Model 2: Dynamic Clump Size.—In the dynamic clump model, it is assumed that an  ${\bf R}$  clump has some initial characteristic length at t=0,  $L_c(0)$  and that strain due to convection in the mush stretches and thins the clump. Heat diffusion occurs from the  ${\bf R}$  clump to  ${\bf M}$  during clump thinning by deformation. The solution of Kellogg and Turcotte (1987) has been modified to treat this problem. The governing differential equation is

$$\frac{\partial T}{\partial t} - \dot{\epsilon}_X = \kappa_R \frac{\partial^2 T}{\partial x^2} \tag{B13}$$

where T(x,t) is the temperature of the clump and the x coordinate is the direction parallel to the width of the clump. The initial conditions are

$$T_R(x) = T(x, 0) = 1 \text{ if } |x| \le L_c(0) \text{ and } 0 \text{ if } |x| > L_c(0)$$
 (B14)

In this model & represents the Lagrangian strain rate induced by the convective motion of the mush. The characteristic length associated with a clump decreases exponentially with time according to:

$$L_c(t) = 2L_c(0) \exp(-\dot{\epsilon}t) \tag{B15}$$

Equation (B13) can be transformed (Ottino, 1989) to eliminate the advective term. After applying a Fourier transform, integrating and then taking the inverse transform and applying the convolution theorem the solution to the original differential equation is:

$$T(x,t) = \frac{1}{2} \operatorname{erf} \left[ \frac{L_c(0) - x e^{\hat{\epsilon}t}}{\left(\frac{2\kappa_R}{\hat{\epsilon}} (e^{2\hat{\epsilon}t} - 1)\right)^{1/2}} \right] + \frac{1}{2} \operatorname{erf} \left[ \frac{L_c(0) + x e^{\hat{\epsilon}t}}{\left(\frac{2\kappa_R}{\hat{\epsilon}} (e^{2\hat{\epsilon}t} - 1)\right)^{1/2}} \right]$$
(B16)

The maximum temperature occurs in the center of the clump, x=0. When the temperature at the center is reduced to within 5% of the thermal equilibration temperature, the clump of R is essentially in thermal equilibrium with host M magma. We define the unlocking condition by:

$$T(0, \tau_{unlock}) = \frac{T_R(\tau_{unlock}) - T_M(0)}{T_R(0) - T_M(0)} = 1/20$$
 (B17)

Using the criterion that  $\mathbf{M}$  is unlocked when the temperature at the center of the clump is  $1/20^{\text{th}}$  of the initial non-dimensional temperature, the unlocking time can be found combining (B15) and (B16):

$$\tau_{\rm unlock} = \frac{1}{2\dot{\epsilon}} \ln \left[ 200 \, \frac{\rho_R C_R^* \, \dot{\epsilon} L_c^2(0)}{k_R} + 1 \right] \tag{B18}$$

which is identical to equation (3) in the text.

TABLE B1

Shape and size of R	Volume of	Characteristic length of
clump	single clump, $v_R$	clump, $L_c = (v_R/a_R)$
Spherical (r = radius)	$\frac{4}{3}\pi r^3$	r/3
Long cylindrical	$\pi \ell r^2$	r/2
conduit ( $\ell >> r$ )		
$(\ell = length)$		
Short cylindrical	$\pi r^3$	r/4
conduit ( $\ell = r$ )		
Rectangular sheet:	$\ell_{ m WZ}$	$\ell_{ m WZ}$
(dike or sill) arbitrary		$\overline{2(\ell z + wz + \ell w)}$
$\ell, w, z$		
(length, width, depth,		
respectively)		
Rectangular sheet:	$w\ell^2$	$\ell^2$ W
(dike or sill)		$\frac{2\ell(\ell+2w)}{2\ell(\ell+2w)}$
$(z = \ell)$		
Rectangular sheet:	$\alpha^2 \text{w}^3$	αw
(dike or sill)		$2(\alpha+2)$
$z = \ell$ and $\ell = \alpha w$ .		
Dike is as long as it is		equals w/2 in limit α large
deep with length $\alpha$		
times its width.		

Table B2

Thermal conductivity of M magma	$k_{M}$
Isobaric heat capacity M magma	$C_{M}$
Thermal expansivity of M magma	$\alpha_{\mathrm{M}}$
Gravity acceleration	g
Temperature difference across M magma body	ΔΤ
Shear viscosity of M magma	η
Volume of M magma body	$V_{\mathrm{M}}$
Volume of R magma	$V_R$
Scaling constant relating convective velocity	$a_1$
to Ra	
M magma thermal diffusivity	$\kappa_{ m M}$
R magma thermal diffusivity	$\kappa_{ m R}$
Unlocking time for M magma	$ au_{unlock}$

## REFERENCES

- Bachmann, O., and Huber, C., 2016, Silicic magma reservoirs in the Earth's crust: American Mineralogist,
- v. 101, n. 11, p. 2377–2404, https://doi.org/10.2138/am-2016-5675 Bachmann, O., Dungan, M. A., and Lipman, P. W., 2002, The Fish Canyon Magma Body, San Juan Volcanic Field, Colorado: Rejuvenation and Eruption of an Upper-Crustal Batholith: Journal of Petrology, v. 43,
- n. 8, p. 1469–1503, https://doi.org/10.1093/petrology/43.8.1469
  Bacon, C. R., and Lowenstern, J. B., 2005, Late Pleistocene granodiorite source for recycled zircon and phenocrysts in rhyodacite lava at Crater Lake, Oregon: Earth and Planetary Science Letters, v. 233, n. 3–4, p. 277–293, https://doi.org/10.1016/j.epsl.2005.02.012 Baxter, S., and Feely, M., 2002, Magma mixing and mingling textures in granitoids: Examples from the
- Galway granite, Connemara, Ireland: Mineralogy and Petrology, v. 76, n. 1-2, p 63-74, https://doi.org/ 10.1007/s007100200032
- Bea, F., Pereira, M. D., and Stroh, A., 1994, Mineral/leucosome trace-element partitioning in a peraluminous migmatite (a laser ablation-ICP-MS study): Chemical Geology, v. 117, n. 1-4, p. 291-312, https://doi.org/10.1016/0009-2541(94)90133-3
- Bernal, J. D., 1959, A geometrical approach to the structure of liquids: Nature, v. 183, p. 141–147, https://doi.org/10.1038/183141a0
- Bird, R. B., Stewart, W. E., and Lightfoot, E. N., 1960, Transport Phenomena: New York, John Wiley and Sons, 780 p
- Bohrson, W. A., Spera, F. J., Ghiorso, M. S., Brown, G. A., Creamer, J. B., and Mayfield, A., 2014, Thermodynamic Model for Energy-Constrained Open-System Evolution of Crustal Magma Bodies Undergoing Simultaneous Recharge, Assimilation and Crystallization: The Magma Chamber Simulator: Journal of Petrology, v. 55, n. 9, p. 1685–1717, https://doi.org/10.1093/petrology/egu036
- Bowen, N. L., 1915, The later stages of the evolution of the igneous rocks: Journal of Geology, v. 23, p. 1–89, https://doi.org/10.1086/622298
- —— 1928, Evolution of the Igneous Rocks: Princeton, New Jersey, Princeton University Press, 334 p.

  Bragagni, A., Avanzinelli, R., Freymuth, H., and Francalanci, L., 2014, Recycling of crystal mush-derived melts and short magma residence times revealed by U-series disequilibria at Stromboli volcano: Earth
- and Planetary Science Letters, v. 404, p. 206–219, https://doi.org/10.1016/j.epsl.2014.07.028

  Brown, S. J. A., and Fletcher, I. R., 1999, SHRIMP U-Pb dating of the preeruption growth history of zircons from the 340 ka Whakamaru Ignimbrite, New Zealand: Evidence for >250 k.y. magma residence times:

  Geology, v. 27, n. 11, p. 1035–1038, https://doi.org/10.1130/0091-7613(1999)027<1035: SUPDOT>2.3.CO;2
- Burgisser A., and Bergantz, G. W., 2011, A rapid mechanism to remobilize and homogenize highly crystalline magma bodies: Nature, v. 471, p. 212–216, https://doi.org/10.1038/nature09799

- Bunsen, R. W., 1851, Uber die processe der vulkanischen Gesteinbildungen Islands: Annotations of Physical Chemistry, v. 83, p. 197–272.
- Carslaw, H. S., and Jaeger, J. C., 1959, Conduction of Heat in Solids: Oxford, England, Oxford University Press, 510 p.
- Claiborne, L. L., Miller, C. F., Flanagan, D. M., Clynne, M. A., and Wooden, J. L., 2010, Zircon reveals protracted magma storage and recycling beneath Mount St. Helens: Geology, v. 38, n. 11, p. 1011–1014, https://doi.org/10.1130/G31285.1
- Coleman, D. S., Gray, W., and Glazner, A. F., 2004, Rethinking the emplacement and evolution of zoned plutons: Geochronologic evidence for incremental assembly of the Tuolumne Intrusive Suite, Califor-
- nia: Geology, v. 32, n. 5, p. 433–436, https://doi.org/10.1130/G20220.1 Coltice, N., and Schmalzl, J., 2006, Mixing times in the mantle of the early Earth derived from 2-D and 3-D numerical simulations of convection: Geophysical Research Letters, v. 33, n. 23, https://doi.org/10.1029/ 2006GL027707
- Cooper, K. M., and Kent, A. J. R., 2014, Rapid remobilization of magmatic crystals kept in cold storage: Nature, v. 506, p. 480–483, https://doi.org/10.1038/nature12991
- Cottrell, E., Spiegelman, and Langmuir, C. H., 2002, Consequences of diffusive reequilibration for the interpretation of melt inclusions: Geochemistry, Geophysics, Geosystems, v. 3, n. 4, p. 1–26, https:// doi.org/10.1029/2001GC000205
- Daly, R. A., 1905, The secondary origin of certain Granites: American Journal of Science, Fourth Series, v. 20, n. 117, p. 185–214, https://doi.org/10.2475/ajs.s4-20.117.185
- 1914, Igneous rocks and their origin: New York, McGraw Hill, 563 p.
- Didier, J., and Barbarin, B., 1991, Enclaves and granite petrology: New York, Elsevier, Developments in Petrology, Book 13, 625 p.
- Druitt, T. H., Costa, F., Deloule, E., Dungan, M., and Scaillet, B., 2012, Decadal to monthly timescales of magma transfer and reservoir growth at a caldera volcano: Nature, v. 482, p. 77–80, https://doi.org/ 10.1038/nature10706
- Eddy, M. P., Bowring, S. A., Miller, R. B., and Tepper, J. H., 2016, Rapid assembly and crystallization of a fossil large-volume silicic magma chamber: Geology, v. 44, n. 4, p. 331–334, https://doi.org/10.1130/ G37631.1
- Ewart, A., and Griffin, W. L., 1994, Application of Proton-Microprobe Data to Trace-Element Partitioning in Volcanic-Rocks: Chemical Geology, v. 117, p. 251–284, https://doi.org/10.1016/0009-2541(94)90131-7
- Finney, J. L., 2013, Bernal's road to random packing and the structure of liquids: Philosophical Magazine,
- v. 93, n. 31–33, p. 3940–3969, https://doi.org/10.1080/14786435.2013.770179

  Fowler, S. J., Spera, F. J., Bohrson, W. A., Belkin, H. E., and De Vivo, B., 2007, Phase Equilibria Constraints on the Chemical and Physical Evolution of the Campanian Ignimbrite: Journal of Petrology, v. 48, n. 3,
- p. 459–493, https://doi.org/10.1093/petrology/egl068

  Furman, T., and Spera, F. J., 1985, Commingling of acid and basic magma and implications for the origin of I-type xenoliths: Field and petrochemical relations of an unusual dike complex at Eagle Lake, Sequoia National Park, Sierra Nevada, California, USA: Journal of Volcanology and Geothermal Research, v. 24, n. 1–2, p. 151–178, https://doi.org/10.1016/0377-0273(85)90031-9

  Ghiorso, M. S., and Gualda, G. A. R., 2015, An H<sub>2</sub>O–CO<sub>2</sub> mixed fluid saturation model compatible with
- rhyolite-MELTS: Contributions to Mineralogy and Petrology, v. 169, n. 6, Article 53, p. 1–30, https://doi.org/10.1007/s00410-015-1141-8
- Gualda, G. A. R., Ghiorso, M. S., Lemons, R. V., and Carley, T. L., 2012, Rhyolite-MELTS: A Modified Calibration of MELTS Optimized for Silica-rich, Fluid-bearing Magmatic Systems: Journal of Petrology, v. 53, n. 5, p. 875–890, https://doi.org/10.1093/petrology/egr080
- Horn, I., Foley, S. F., Jackson, S. E., and Jenner, G. A., 1994, Experimentally determined partitioning of high
- field strength- and selected transition elements between spinel and basaltic melt: Chemical Geology, v. 117, n. 1–4, p. 193–218, https://doi.org/10.1016/0009-2541(94)90128-7

  Huber, C. O., Bachmann O., and Dufek, J., 2010, The limitations of melting on the reactivation of silicic mushes: Journal of Volcanology and Geothermal Research, v. 195, n. 2–4, p. 97–105, https://doi.org/ 10.1016/j.jvolgeores.2010.06.006
- Huber, C., Bachmann, O., and Dufek, J., 2011, Thermo-mechanical reactivation of locked crystal mushes: Melting-induced internal fracturing and assimilation processes in magmas: Earth and Planetary Science Letters, v. 304, n. 34, p. 443–454, https://doi.org/10.1016/j.epsl.2011.02.022
- Ingersol, L. R., Zobel, O. J., and Ingersoll, A. C., 1948, Heat Conduction with Engineering and Geological
- applications: New York, McGraw-Hill Book Company, 278 p.
  Kaviany, M., 2002, Principles of Heat Transfer: New York, John Wiley & Sons, Inc., 1000 p.
  Kellogg, L. H., and Turcotte, D. L., 1986/87, Homogenization of the mantle by convective mixing and diffusion: Earth and Planetary Science Letters, v. 81, n. 4, p. 371–378, https://doi.org/10.1016/0012-821X(87)90124-5
- 1990, Mixing and the distribution of heterogeneities in a chaotically convecting mantle: Journal of Geophysical Research, v. 95, p. 421–432, https://doi.org/10.1029/JB095iB01p00421 Klemetti, E. W., and Clynne, M. A., 2014, Localized Rejuvenation of a Crystal Mush Recorded in Zircon
- Temporal and Compositional Variation at the Lassen Volcanic Center, Northern California: PLoS ONE,
- v. 9, n. 12, https://doi.org/10.1371/journal.pone.0113157.0113157

  Klemetti, E. W., Deering, C. D., Cooper, K. M., and Roeske, S. M., 2011, Magmatic perturbations in the Okataina Volcanic Complex, New Zealand at thousand-year timescales recorded in single zircon crystals: Earth and Planetary Science Letters, v. 305, n. 1–2, p. 185–194, https://doi.org/10.1016/ j.epsl.2011.02.054
- Klemme, S., and Dalpé, C., 2003, Trace element partitioning between apatite and carbonatite melt: American Mineralogist, v. 88, n. 4, p. 639-646, https://doi.org/10.2138/am-2003-0417

- Klemme, S., Günther, D., Hametner, K., Prowatke, S., and Zack, T., 2006, The partitioning of trace elements between ilmenite, ulvospinel, armalcolite and silicate melts with implications for the early differentiation of the moon: Chemical Geology, v. 234, n. 3-4, p. 251-263, https://doi.org/10.1016/ j.chemgeo.2006.05.005
- Lesher, C. E., and Spera, F. J., 2015, Thermodynamic and Transport Properties of Silicate Melts and Magma, in Sigurdsson, H., Houghton, B., Rymer, H., Stix, J., and McNutt, S, editors, The Encyclopedia of Volcanoes: Amsterdam, Academic Press, p. 113–141, https://doi.org/10.1016/B978-0-12-385938-9.00005-5
- Madruga, S., and Curbelo, J., 2017, Dynamics of plumes and scaling during melting of a Phase Change Material heated from below: eprint arXiv:1711.07744, November, 2017.
- Mahood, G. A., 1990, Second reply to comment of R.S.J. Sparks, H.E. Huppert, and C.J.N. Wilson on 'Evidence for long residence times of rhyolitic magma in the Long Valley magmatic system: The isotopic record in precaldera lavas of Glass Mountain': Earth and Planetary Science Letters, v. 99, n. 4,
- p. 395–399, https://doi.org/10.1016/0012-821X(90)90145-N Mahood, G. A., and Hildreth, W., 1983, Large partition coefficients for trace elements in high-silica rhyolites: Geochimica et Cosmochimica Acta, v. 47, n. 1, p. 11-30, https://doi.org/10.1016/0016-7037(83)90087-X
- Mahood, G. A., and Stimac, J. A., 1990, Trace-element partitioning in pantellerites and trachytes: Geochimica et Cosmochimica Acta, v. 54, n. 8, p. 2,257–2,276, https://doi.org/10.1016/0016-7037(90)90050-U
- Marsh, B. D., 1981, On the crystallinity, probability of occurrence, and rheology of lava and magma:
- Contributions to Mineralogy and Petrology, v. 78, n. 1, p. 85–98, https://doi.org/10.1007/BF00371146
  Matthews, N. E., Pyle, D. M., Smith, V. C., Wilson, C. J. N., Huber, C., and van Hinsberg, V., 2011, Quartz zoning and the pre-eruptive evolution of the ~340-ka Whakamaru magma systems, New Zealand: Contributions to Mineralogy and Petrology, v. 163, n. 1, p. 87–107, https://doi.org/10.1007/s00410-011-
- Matthews, N. E., Huber, C., Pyle, D. M., and Smith, V. C., 2012, Timescales of Magma Recharge and Reactivation of Large Silicic Systems from Ti Diffusion in Quartz: Journal of Petrology, v. 53, n. 7,
- p. 1385–1416, https://doi.org/10.1093/petrology/egs020

  Miller, C. F., and Wark, D. A., 2008, Supervolcanoes and Their Explosive Supereruptions: Elements, v. 4, n. 1, p. 11–15, https://doi.org/10.2113/GSELEMENTS.4.1.11
- Miller, J. S., Matzel, J. E. P., Miller, C. F., Burgess, S. D., and Miller, R. B., 2007, Zircon growth and recycling during the assembly of large, composite arc plutons: Journal of Volcanology and Geothermal Research,
- v. 167, n. 14, p. 282–299, https://doi.org/10.1016/j.jvolgeores.2007.04.019

  Moitra, P., and Gonnermann, H. M., 2015, Effects of crystal shape- and size-modality on magma rheology:
  Geochemistry, Geophysics, Geosystems, v. 16, n. 1, p. 1–26, https://doi.org/10.1002/2014GC005554
- Molloy, C., Shane, P., and Nairn, I., 2008, Pre-eruption thermal rejuvenation and stirring of a partly crystalline pluton revealed by the Earthquake Flat Pyroclastics deposits, New Zealand: Journal of the Geological Society, v. 165, n. 1, p. 435–447, https://doi.org/10.1144/0016-76492007-071
- Nakamura, M., 1995, Continuous mixing of crystal mush and replenished magma in the ongoing Unzen eruption: Geology, v, 23, n. 9, p. 807–810, https://doi.org/10.1130/0091-7613(1995)023<0807: CMOCMA>2.3.CO;2
- Nash, W. P., and Crecraft, H. R., 1985, Partition coefficients for trace elements in silicic magmas: Geochimica
- et Cosmochimica Acta, v. 49, n. 11, p. 2,309–2,322, https://doi.org/10.1016/0016-7037(85)90231-5 Olson, P., Yuen, D. A., and Balsiger, D., 1984, Mixing of passive heterogeneities by mantle convection: Journal of Geophysical Research, v. 89, n. B1, p. 425–436, https://doi.org/10.1029/JB089iB01p00425
- Ottino, J. M., 1989, The kinematics of mixing: stretching, chaos and transport: Cambridge, United Kingdom, Cambridge University Press, 364 p.
- Pabst, A., 1928, Observations on inclusions in the granitic rocks of the Sierra Nevada: University of California Publications, v. 17, p. 325–386.
  Pallister, J. S., Hoblitt, R. P., and Reyes, A. G., 1992, A basalt trigger for the 1991 eruptions of Pinatubo
- Volcano?: Nature, v. 356, p. 426–428, https://doi.org/10.1038/356426a0
  Pamukcu, A. S., Gualda, G. A. R., Bégué, F., and Gravley, D. M., 2015, Melt inclusion shapes: Timekeepers of
- short-lived giant magma bodies: Geology, v. 43, n. 11, p. 947–950, https://doi.org/10.1130/G37021.1 Parmigiani, A., Huber, C., and Bachmann, O., 2014, Mush microphysics and the reactivation of crystal-rich
- magma reservoirs: Journal of Geophysical Research-Solid Earth, v. 119, n. 8, https://doi.org/10.1002/ (ISSN)2169-9356
- Pistone, M., Caricchi, L., Ulmer, P., Reusser, E., and Ardia, P., 2013, Rheology of volatile-bearing crystal mushes: Mobilization vs. viscous death: Chemical Geology, v. 345, p. 16–39, https://doi.org/10.1016/ j.chemgeo.2013.02.007
- Philpotts, J. A., and Schnetzler, C. C., 1970, Phenocryst-matrix partition coefficients for K, Rb, Sr and Ba, with applications to anorthosite and basalt genesis: Geochimica et Cosmochimica Acta, v. 34, n. 3, p. 307–322, https://doi.org/10.1016/0016-7037(70)90108-0
- Reid, J. B., Jr., Evans, O. C., and Fates, D. G., 1983, Magma mixing in granitic rocks of the central Sierra Nevada, California: Earth and Planetary Science Letters, v. 66, p. 243–261, https://doi.org/10.1016/ 0012-821X(83)90139-5
- Schmitt, A. K., 2006, Laacher See revisited: High-spatial-resolution zircon dating indicates rapid formation of
- a zoned magma chamber: Geology, v. 34, n. 7, p. 597–600, https://doi.org/10.1130/G22533.1 Schneider, P. J., 1955, Conduction Heat Transfer: Reading, Massachusetts, Addison-Wesley Publishing Co., Inc., 395 p.
- Sinton, J. M., and R. S. Detrick, 1992, Mid-ocean ridge magma chambers: Journal of Geophysical Research-Solid Earth, v. 97, n. B1, p. 197–216, https://doi.org/10.1029/91JB02508
- Spera, F. J., 1992, Lunar magma transport phenomena: Geochimica et Cosmochimica Acta v. 56, n. 6, p. 2253–2265, https://doi.org/10.1016/0016-7037(92)90187-N

- Spera, F. J., Bohrson, W. A., Till, C. B., and Ghiorso, M. S., 2007, Partitioning of trace elements among coexisting crystals, melt, and supercritical fluid during isobaric crystallization and melting: American Mineralogist, v. 92, n. 11–12, p. 1881–1898, https://doi.org/10.2138/am.2007.2326
- Spera, F. J., Schmidt, J. S., Bohrson, W. A., and Brown, G. A., 2016, Dynamics and thermodynamics of magma mixing: Insights from a simple exploratory model: American Mineralogist, v. 101, n. 3, p. 627–643, https://doi.org/10.2138/am-2016-5305
- Stix, J., and Gorton, M. P., 1990, Variations in Trace-Element Partition-Coefficients in Sanidine in the Cerro Toledo Rhyolite, Jemez Mountains, New-Mexico-Effects of Composition, Temperature, and Volatiles: Geochimica et Cosmochimica Acta, v. 54, n. 10, p. 2,697–2,708, https://doi.org/10.1016/0016-7037(90)90005-6
- Streck, M. J., 2014, Evaluation of crystal mush extraction models to explain crystal-poor rhyolites: Journal of Volcanology and Geothermal Research, v. 284, p. 79–94, https://doi.org/10.1016/j.jvolgeores.2014.07.005
- Streck, M. J., and Grunder, A. L., 1997, Compositional gradients and gaps in high-silica rhyolites of the Rattlesnake Tuff, Oregon: Journal of Petrology, v. 38, n. 1, p. 133–163, https://doi.org/10.1093/petroj/38 1 133
- Till, C. B., Vazquez, J. A., and Boyce, J. W., 2015, Months between rejuvenation and volcanic eruption at Yellowstone caldera, Wyoming: Geology, v. 43, n. 8, p. 695–698, https://doi.org/10.1130/C36862.1
- Vazquez, J. A., and Reid, M. R., 2004, Probing the Accumulation History of the Voluminous Toba Magma: Science, v. 305, n. 5686, p. 991-994, https://doi.org/10.1126/science.1096994
- Vernon, R. H., 1990, Crystallization and hybridism in microgranitoid enclave magmas: Microstructural evidence: Journal of Geophysical Research, v. 95, n. B11, p. 17849–17859, https://doi.org/10.1029/JB095iB11p17849
- Wark, D. A., Hildreth, W., Spear, F. S., Cherniak, D. J., and Watson, E. B., 2007, Pre-eruption recharge of the Bishop magma system: Geology, v. 35, n. 3, p. 235–238, https://doi.org/10.1130/G23316A.1 Watson, E. B., and Green, T. H., 1981, Apatite/liquid partition coefficients for the rare earth elements and
- Watson, E. B., and Green, T. H., 1981, Apatite/liquid partition coefficients for the rare earth elements and strontium: Earth and Planetary Science Letters, v. 56, p. 405–421, https://doi.org/10.1016/0012-821X(81)90144-8
- Wiebe, R. A., 1996, Mafic-silicic layered intrusions: The role of basaltic injections on magmatic processes and the evolution of silicic magma chambers: Geological Society of America, Special Papers, v. 315, p. 233–242, https://doi.org/10.1130/0-8137-2315-9.233
- Wiebe, R. A., Manon, M. R., Hawkins, D. P., and McDonough, W. F., 2004, Late-Stage Mafic Injection and Thermal Rejuvenation of the Vinalhaven Granite, Coastal Maine: Journal of Petrology, v. 45, n. 11, p. 2133–2153, https://doi.org/10.1093/petrology/egh050
- Wilcox, R. E., 1999, The idea of magma mixing: History of a struggle for acceptance: The Journal of Geology, v. 107, n. 4, p. 421–432, https://doi.org/10.1086/314357
  Wotzlaw, J. F., Schaltegger, U., Frick, D. A., Dungan, M. A., Gerdes, A., and Günther, D., 2013, Tracking the
- Wotzlaw, J. F., Schaltegger, U., Frick, D. A., Dungan, M. A., Gerdes, A., and Günther, D., 2013, Tracking the evolution of large-volume silicic magma reservoirs from assembly to supercruption: Geology, v. 41, n. 8, p. 867–870, https://doi.org/10.1130/G34366.1
- Zellmer, G. F., Sparks, R. J. S., Hawkesworth, C. J., and Wiedenbeck, M., 2003, Magma Emplacement and Remobilization Timescales Beneath Montserrat: Insights from Sr and Ba Zonation in Plagioclase Phenocrysts: Journal of Petrology, v. 44, n. 8, p. 1413–1431, https://doi.org/10.1093/petrology/ 44.8.1413